Journal of Molecular Liquids 267 (2018) 520–541

Contents lists available at ScienceDirect

Journal of Molecular Liquids

journal homepage: www.elsevier.com/locate/molliq

Introduction to liquid crystals

Denis Andrienko

Max Planck Institute for Polymer Research, Ackermannweg 10, 55128 Mainz, Germany

ARTICLE INFO

Article history:
Received 6 November 2017
Received in revised form 20 January 2018
Accepted 30 January 2018
Available online 3 February 2018

ABSTRACT

This pedagogical overview of liquid crystals is based on lectures for postgraduate students given at the International Max Planck Research School "Modeling of Soft Matter". I am delighted to dedicate it to my scientific advisor, Prof. Yuriy Reznikov, thus acknowledging his valuable contribution to my life.

1. Literature

Many excellent books and reviews cover different aspects of liquid crystals. The compilation below is far from being complete and curious readers should take it as a starting point only.

1. The "gold standard" reference on liquid crystals: P. G. de Gennes and J. Prost "The Physics of Liquid Crystals" [1].
2. Excellent review of basic properties (many topics are taken from this review): M. J. Stephen, J. P. Straley "Physics of liquid crystals" [2].
3. Symmetries, hydrodynamics, theory: P. M. Chaikin and T. C. Lubensky "Principles of Condensed Matter Physics" [3].
4. Defects: O. D. Lavrentovich and M. Kleman, "Defects and Topology of Cholesteric Liquid Crystals" [4]; Oleg Lavrentovich "Defects in Liquid Crystals: Computer Simulations, Theory and Experiments" [5].
5. Optics: Iam-Choon Khoo, Shin-Tson Wu, "Optics and Nonlinear Optics of Liquid Crystals" [6].
6. Textures: Ingo Dierking "Textures of Liquid Crystals" [7].
7. Simulations: Michael P. Allen and Dominic J. Tildesley "Computer simulation of liquids" [8].
8. Phenomenological theories: Epifanio G. Virga "Variational Theories for Liquid Crystals" [9].
9. History: David Dunmur and Tim Sluckin "Soap, science, and flat-screen TVs: A history of liquid crystals" [10].

2. What is a liquid crystal?

The notion of a state of matter which is liquid-like and crystalline at the same time seems absurd. It is, however, fully justified: liquid crystalline mesophases possess some typical properties of a liquid, such as fluidity and the inability to support shear, formation and coalescence of droplets. These mesophases also have certain crystalline properties, such as anisotropy of optical, electrical, and magnetic properties, as well as a periodic arrangement of molecules in one or more spatial directions.

Depending on the arrangement of the molecules in a mesophase, or its symmetry, liquid crystals are subdivided into nematics, cholesterics, smectics, and columnar mesophases. Molecular arrangements of these mesophases are depicted in Fig. 1.

2.1. Nematics

In a nematic mesophase molecules possess a long-range orientational order with molecular long axes aligned along a preferred direction. There is no long-range order in the positions of centers of mass of molecules. The preferred direction may vary throughout the medium and is called a director. The orientation of the director is represented by a unit vector, $\boldsymbol{n}(\boldsymbol{r})$. In a nematic, the molecules are able to rotate around their long axes, and there is no preferential arrangement of their ends, even if they differ. Hence, the sign of the director has no physical significance, and the nematic behaves optically as a uniaxial material with a center of symmetry. We will introduce a mathematically rigorous definition of the director in Section 4. The director and the molecular arrangement in a nematic mesophase are sketched in Fig. 1, where the anisotropic shape of molecules is depicted by ellipses.

While optically examining a nematic mesophase, we rarely observe the idealized uniform equilibrium configuration of the director. Fig. 2 (a) is an example of a schlieren texture of a nematic taken using a microscope with crossed polarizers. Here, four dark brushes emerge from every point-defect indicating that the director is parallel to the polarizer or analyzer. The colors are Newton colors of thin films and depend on the thickness of the sample. Since

E-mail address: denis.andrienko@mpip-mainz.mpg.de.

https://doi.org/10.1016/j.molliq.2018.01.175
0167-7322/

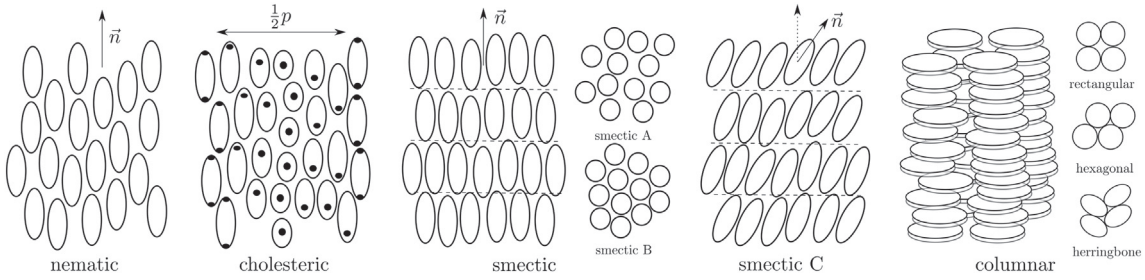

Fig. 1. Molecular arrangements in liquid crystalline mesophases. In a *nematic* mesophase, molecular orientations are correlated, while molecular positions are not. The average orientation is termed a director, $\boldsymbol{n}$. In a *cholesteric* mesophase the average molecular orientation twists through the medium with a certain periodicity, while positions of molecules are not correlated. In a *smectic A* mesophase molecules lie in planes. Molecular axes are perpendicular to these planes but otherwise are not ordered within the planes. *Smectic B* has a hexagonal packing of molecules in the planes, while in *smectic C* the director is tilted in the planes. *Columnar* mesophases are often formed by disc-shaped molecules. The most common arrangements of columns in two-dimensional lattices are hexagonal, rectangular, and herringbone. In the herringbone mesophase molecules are tilted with respect to the columnar axis.

point defects can only exist in pairs, two types of defects can be seen: the first one has yellow and red brushes and the second one is less colorful. The difference in appearance is due to different cores and opposite signs of their topological charges, which are discussed later in Section 12. The texture in Fig. 2 (b) is a photo of a thin nematic film on an isotropic surface. Here the periodic stripes arise from the competition between bulk elastic and surface anchoring forces in a confined film. The surface anchoring aligns molecules parallel to the bottom surface and perpendicular to the top surface of the film. The elastic forces work against the distortions of the director field. When the film is sufficiently thin, the lowest energy state corresponds to the director in the plane of the film. The pattern in Fig. 2 (c) shows a thread-like texture. Threads are analogous to dislocations in solids and are referred to as *disclinations*. Nematics owe their name to these defects: the Greek word "$\nu\eta\mu\alpha''$ stands for thread.

From a chemical point of view, molecules forming nematic crystalline mesophases have anisotropic shapes, often with rigid molecular backbones which define the long axes of molecules. Liquid crystallinity is more likely to occur if molecules have flat segments, e. g. benzene rings. Many liquid crystalline compounds have strong dipole moments and easily polarizable groups. Typical compounds forming nematics are shown in Fig. 3.

2.2. Cholesterics

The cholesteric mesophase is similar to the nematic: it has a long-range orientational order, but no long-range positional order of the centers of mass of molecules. It differs from the nematic mesophase in that the director varies throughout the medium in a regular way even in an unstrained state. The director distribution is precisely what would be obtained by twisting a nematic aligned along the y axis about the x axis. In any plane perpendicular to the twist axis the long axes of the molecules align along a single preferred direction in this plane, but in a series of parallel planes this direction rotates uniformly, as illustrated in Fig. 1. The secondary structure of the cholesteric is characterized by the distance measured along the twist axis over which the director rotates through a full circle. This distance is called the pitch of the cholesteric, p. The periodicity length of the cholesteric is actually only a half of this distance, since $\boldsymbol{n}$ and $-\boldsymbol{n}$ are indistinguishable.

Formally, a nematic liquid crystal is a cholesteric of an infinite pitch. As a result, there is no phase transition between nematic and cholesteric mesophases: nematics doped with enantiomorphic compounds become cholesterics of long but finite pitch. The molecules forming the cholesteric mesophase have distinct right- and left-handed forms, as illustrated in Fig. 3.

The pitch of common cholesterics is of the order of several hundreds nanometers, which is comparable to the wavelength of visible light. Through Bragg reflection, the periodic spiral arrangement is responsible for the characteristic colors of cholesterics in reflection and their very large rotatory power. The pitch can be quite sensitive to temperature, flow, chemical composition, and applied magnetic or electric fields [11]. Typical cholesteric textures are shown in Fig. 2.

2.3. Smectics

The important feature of a smectic mesophase, which distinguishes it from a nematic or a cholesteric one, is its stratification. The molecules are arranged in layers and exhibit some correlations in their positions in addition to the orientational ordering. The layers can slide freely over one another. Depending on the molecular order in layers, a number of different types of smectics have been observed. In a smectic A, molecules are aligned perpendicular to the layers, without long-range crystalline ordering within them, as shown in Fig. 1. In a smectic C, the preferred molecular axis is not perpendicular to the layers, so that the phase has biaxial symmetry. In a smectic B, there is a hexagonal crystalline order within the layers.

When placed between glass substrates, smectics do not assume the simple arrangement shown in Fig. 1. To preserve their thickness, the layers become distorted and can slide over one another in order to accommodate the substrates. The smectic focal conic texture appears due to these distortions. Typical textures formed by smectics are shown in Fig. 2.

A number of compounds have both nematic (or cholesteric) and smectic mesophases. As a general rule, the lower temperature phases have a greater degree of crystalline order. The nematic mesophase always occurs at a higher temperature than the smectic one; smectic mesophases occur in the following order: A $\rightarrow$ C $\rightarrow$ B as the temperature decreases.

2.4. Columnar mesophases

The columnar mesophase is a class of liquid-crystalline phases in which molecules assemble into cylindrical structures. Originally, these liquid crystals were called discotic liquid crystals because the columnar structures are composed of stacked flat-shaped discotic molecules, such as triphenylene derivatives shown in Fig. 3. Since

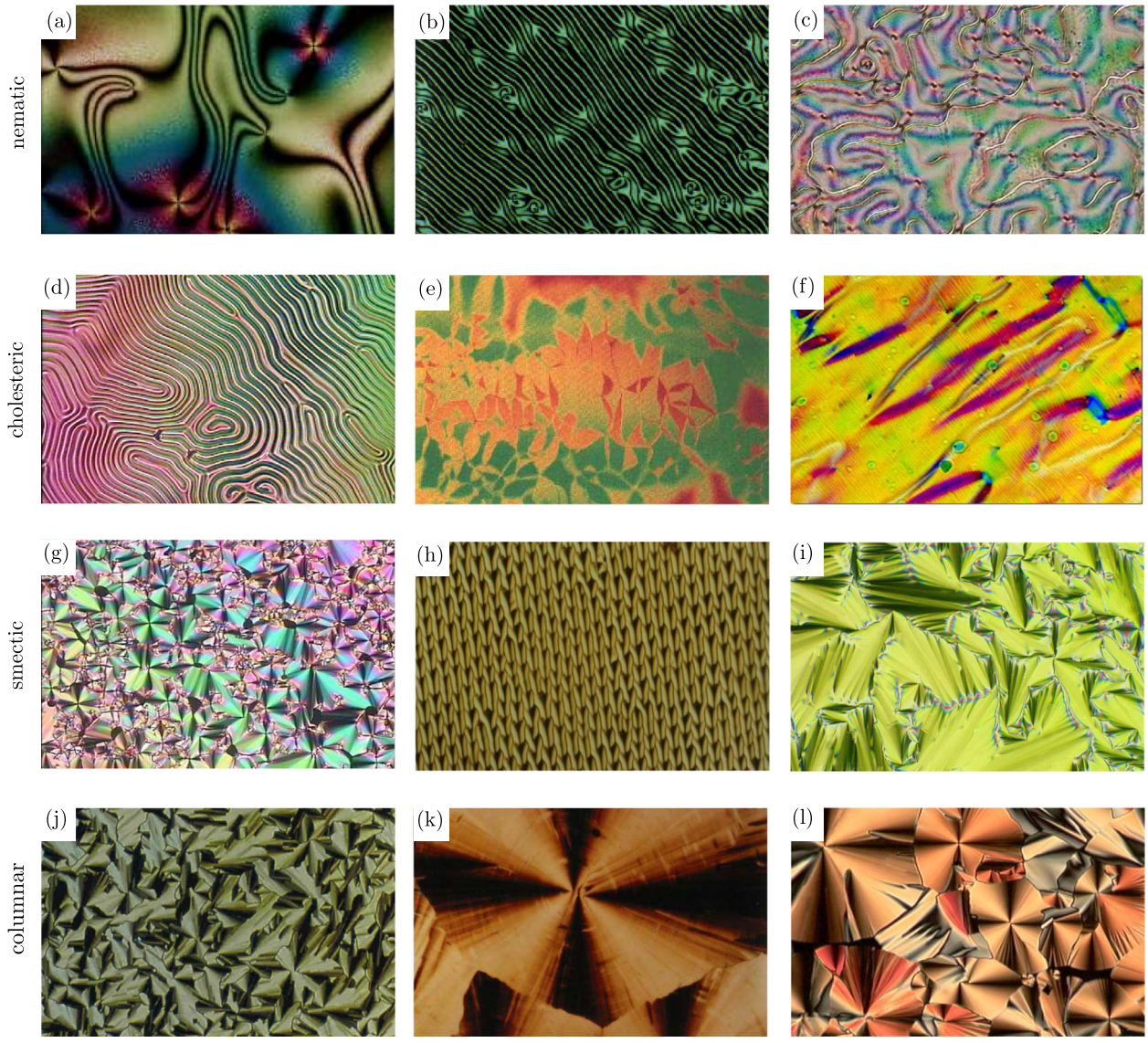

Fig. 2. Liquid crystalline artwork. Nematics: (a) Schlieren texture of a nematic film with surface point defects. (b) Thin nematic film on an isotropic surface. (c) Nematic thread-like texture. Nematic is the Greek word for "thread" observed on these textures. (d) Cholesteric fingerprint texture. The line pattern is due to the helical structure of the cholesteric phase, with the helical axis in the plane of the substrate. (e) A short-pitch cholesteric liquid crystal in Grandjean or standing helix texture, viewed between crossed polarizers. The bright colors are due to the difference in rotatory power arising from domains with different cholesteric pitches. This pattern occurs upon rapid cooling close to the smectic A* phase, where the pitch strongly diverges with decreasing temperature. (f) Long-range orientation of cholesteric liquid crystalline DNA mesophases in a magnetic field. (g, h) Focal conic texture of a chiral smectic A liquid crystal. (i) Focal conic texture of a chiral smectic C liquid crystal. (j) Hexagonal columnar phase with a typical spherulitic texture. (k) Rectangular phase of a discotic liquid crystal. (l) Hexagonal columnar liquid-crystalline phase.
Source: Photos courtesy of Oleg Lavrentovich (http://www.lavrentovichgroup.com/textures.html), Ingo Dierking (http://softmatter-_dierking.myfreesites.net), Per Rudqvist, Sivaramakrishna Chandrasekhar, Prasad Krishna, Nair Gita, and Jon Rourke (https://www2.warwick.ac.uk/fac/sci/chemistry/research/rourke/rourkegroup/mesogens/).

recent findings provide a number of columnar liquid crystals consisting of non-discoid mesogens, this state of matter is now classified as columnar liquid crystals [12].

Columnar liquid crystals are grouped according to the packing motive of the columns. In columnar nematics, for example, molecules do not form columnar assemblies but only float with their short axes parallel to each other. In other columnar liquid crystals columns are arranged in two-dimensional lattices: hexagonal, tetragonal, rectangular, and herringbone, as shown in Fig. 1.

2.5. Lyotropic liquid crystals

Liquid crystals, which are obtained by melting a crystalline solid, are called *thermotropic*. Liquid crystalline behavior is also found in certain colloidal solutions, such as aqueous solutions of tobacco mosaic virus and certain polymers. This class of liquid crystals is called *lyotropic*. For lyotropic liquid crystals the important controllable parameter is the concentration, rather than temperature or pressure. Most of the theories presented below are equally valid for thermotropic and lyotropic liquid crystals. Generally, we will have a thermotropic liquid crystal in mind as a basis for discussion.

3. Order tensor

To quantify the degree of molecular ordering at a specific position as well as the change of the average molecular orientation in space, we need to introduce local averages over the distribution of molecular orientations. The orientation of a rigid, rod-like molecule

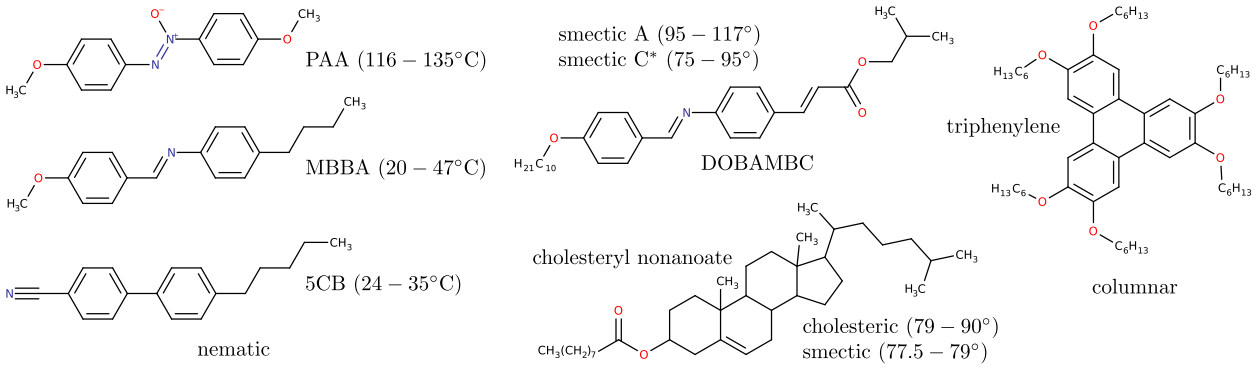

Fig. 3. Typical compounds forming nematic, cholesteric, smectic, and columnar mesophases. Nematics: *p*-azoxyanisole (PAA). From a rough steric point of view it is a rigid rod of length ∼20 Å and width ∼5 Å. The nematic state is found at high temperatures, between 116°C and 135°C. *N*-(*p*-methoxybenzylidene)-*p*-butylaniline (MMBA). The nematic state is found at room temperatures, from 20°C to 47°C. This compound is chemically not very stable. 4-pentyl-4′-cyanobiphenyl (5CB). The nematic state is found at room temperatures, between 24°C and 35°C. Typical cholesteric: [10,13-dimethyl-17-(6-methylheptan-2-yl)-2,3,4,7,8,9,11,12,14,15,16,17-dodecahydro-1H cyclopenta[a]phenanthren-3-yl] nonanoate (cholesteryl nonanoate) with a cholesteric phase between 79°C and 90°C. Typical columnar: 2,3,6,7,10,11-hexakishexyloxytriphenylene (triphenylene derivative) has crystalline, columnar (70–100 °C), and isotropic mesophases.

is uniquely described by a unit vector $\boldsymbol{u}^{(i)}$ along its long axis, as depicted in Fig. 4. Since molecules possess a center of symmetry, the average of the vector $\boldsymbol{u}^{(i)}$ vanishes. It is, therefore, not possible to introduce a *vector* as an order parameter, as it is done to describe the magnetization of a ferromagnet. The next invariant which can be used as an order parameter is the second rank tensor

$$Q_{\alpha\beta}(\boldsymbol{r}) = \frac{1}{N}\sum_i \left(u_\alpha^{(i)} u_\beta^{(i)} - \frac{1}{3}\delta_{\alpha\beta}\right), \tag{1}$$

where the sum is performed over N molecules in a small but macroscopic volume located at the point $\boldsymbol{r}$. The indices α and β denote the Cartesian coordinates x, y, and z.

The tensorial order parameter has a number of useful properties:

1. $Q_{\alpha\beta}$ is symmetric. Indeed, $Q_{\alpha\beta} = Q_{\beta\alpha}$ since $u_\alpha^{(i)} u_\beta^{(i)} = u_\beta^{(i)} u_\alpha^{(i)}$ and $\delta_{\alpha\beta} = \delta_{\beta\alpha}$.
2. It is traceless,

$$\mathrm{Tr}Q_{\alpha\beta} = Q_{xx} + Q_{yy} + Q_{zz} = \\ = \frac{1}{N}\sum_i \left[\left(u_x^{(i)}\right)^2 + \left(u_y^{(i)}\right)^2 + \left(u_z^{(i)}\right)^2 - 1\right] = 0,$$

since $\boldsymbol{u}$ is a unit vector. These two symmetries reduce the number of independent components from 9 to 5.

3. In the isotropic phase $Q_{\alpha\beta}^{\mathrm{iso}} = 0$.
To prove this, let us change to the spherical coordinate system,

$$u_x = \sin\theta\cos\phi,$$
$$u_y = \sin\theta\sin\phi,$$
$$u_z = \cos\theta.$$

Then

$$Q_{\alpha\beta} = \int_0^{2\pi} d\phi \int_0^{\pi} \sin\theta d\theta f(\theta,\phi)\left(u_\alpha u_\beta - \frac{1}{3}\delta_{\alpha\beta}\right),$$

where $f(\theta,\phi)$ is the probability to find a molecule with the orientation given by the angles θ, ϕ. In the isotropic phase $f_{\mathrm{iso}}(\theta,\phi) = 1/4\pi$ and therefore $Q_{xx} = Q_{yy} = Q_{xy} = Q_{zy} = 0$ because of the periodic in ϕ functions integrated over their full periods. For the Q_{zz} component we obtain

$$Q_{zz} = \frac{1}{4\pi}\int_0^{2\pi} d\phi \int_0^{\pi} \sin\theta d\theta \left(\cos^2\theta - \frac{1}{3}\right) = \\ = \frac{1}{6}\left(x^3 - x\right)\Big|_{-1}^{1} = 0.$$

4. In a perfectly aligned prolate nematic with all molecules oriented along the z axis, as shown in Fig. 4, the order tensor takes the form

$$\boldsymbol{Q}^{\mathrm{prolate}} = \begin{pmatrix} -1/3 & 0 & 0 \\ 0 & -1/3 & 0 \\ 0 & 0 & 2/3 \end{pmatrix}.$$

Indeed, $Q_{zz} = u_z u_z - 1/3 = 1 - 1/3 = 2/3$, and $Q_{xx} = Q_{yy} = -1/3$ since $\boldsymbol{Q}$ is traceless.

5. In an oblate case, molecules are randomly oriented perpendicular to the z axis, as depicted in Fig. 4. As a result, $u_z = 0$ and the order tensor simplifies to

$$\boldsymbol{Q}^{\mathrm{oblate}} = \begin{pmatrix} 1/6 & 0 & 0 \\ 0 & 1/6 & 0 \\ 0 & 0 & -1/3 \end{pmatrix}.$$

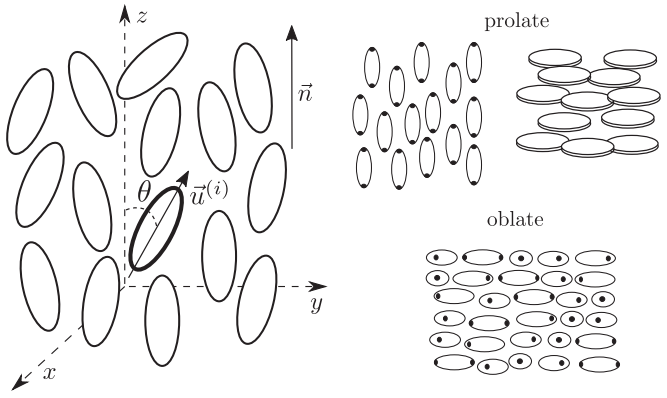

Fig. 4. Orientation of mesogens in a nematic mesophase. A unit vector $\boldsymbol{u}^{(i)}$ along the axis of i-th molecule describes its orientation. The director $\boldsymbol{n}$ corresponds to the average molecular alignment. Two molecular arrangements are shown: ideal prolate, with all molecules aligned along the z axis, and oblate, with molecular axes uniformly distributed in the xy plane.

4. The director and the scalar order parameter

The five independent components of the order tensor often lack clear physical interpretation. In certain cases we can simplify this tensorial object and introduce more intuitive and physically tractable quantities. Indeed, a symmetric second-order tensor has three real eigenvalues and three corresponding orthogonal eigenvectors. A Cartesian coordinate system can be found in which this tensor is diagonal, with the diagonal elements λ_1, λ_2, and $-\lambda_1-\lambda_2$. Let us order the eigenvalues according to their absolute values. The eigenvector with the largest absolute eigenvalue we will call a *director*, $\boldsymbol{n}$. The corresponding eigenvalue, S, is the scalar order parameter.

The order tensor can now be written in the form

$$Q_{\alpha\beta} = S\left(n_\alpha n_\beta - \frac{1}{3}\delta_{\alpha\beta}\right) + B(l_\alpha l_\beta - m_\alpha m_\beta),$$

where B is the biaxiality of the molecular distribution, and the unit vectors $\boldsymbol{l}$, $\boldsymbol{n}$, and $\boldsymbol{m}$ form a local orthonormal triad.

In a *uniaxial* nematic, the molecular distribution function is axially symmetric, the two smaller eigenvalues are equal, $B = 0$, and the order tensor simplifies to

$$Q_{\alpha\beta} = S\left(n_\alpha n_\beta - \frac{1}{3}\delta_{\alpha\beta}\right), \tag{2}$$

where n_α are the components of the director $\boldsymbol{n}$ in a laboratory (fixed) coordinate system.

If we choose $\boldsymbol{n}$ along the z axis of the coordinate system, the three nonzero components of the order tensor become

$$Q_{zz} = \frac{2}{3}S, \qquad Q_{xx} = Q_{yy} = -\frac{1}{3}S.$$

Hence, the scalar quantity S measures the degree of a local molecular alignment. Quantitatively, if $f(\theta)\sin\theta d\theta$ is the fraction of molecules whose axes make angles between θ and $\theta + \Delta\theta$ with the preferred direction, then

$$S = \int_0^\pi \left(1 - \frac{3}{2}\sin^2\theta\right) f(\theta)\sin\theta d\theta, \tag{3}$$

where $f(\theta) = \int_0^{2\pi} f(\theta,\phi)d\phi$.

Uniaxial liquid crystalline mesophases, such as nematics and cholesterics, can therefore be characterized by the scalar order parameter $S(\boldsymbol{r})$ and the director orientation $\boldsymbol{n}(\boldsymbol{r})$. In the isotropic phase $S = 0$, while in the nematic or cholesteric phases $-\frac{1}{2} \le S \le 1$. $S = 1$ corresponds to a perfect prolate alignment, while $S = -\frac{1}{2}$ corresponds to an ideal oblate orientation of mesogens. Both oblate and prolate molecular arrangements are depicted in Fig. 4.

5. Landau–de Gennes free energy

With the appropriate order parameter at hand we can assume, in the spirit of Landau theories, that the free energy density is an analytic function of the order parameter tensor $Q_{\alpha\beta}$. The excess of this free energy with respect to the isotropic phase, g, can therefore be expanded in a power series of $Q_{\alpha\beta}$. Such expansions are justified near the nematic-isotropic transition temperature, where $\boldsymbol{Q}$ is small. Since the free energy is invariant under rigid rotations, all terms of the expansion must be scalar functions of the tensor $Q_{\alpha\beta}$. This tensor has three independent invariants, $\mathrm{Tr}(\boldsymbol{Q}) = 0$, $\mathrm{Tr}(\boldsymbol{Q}^2)$, and $\det(\boldsymbol{Q})$. Expanding g in terms of these invariants up to the fourth order gives

$$\begin{aligned} g &= \frac{A}{2}\mathrm{Tr}(\boldsymbol{Q}^2) - \frac{B}{3}\mathrm{Tr}(\boldsymbol{Q}^3) + \frac{A}{4}\mathrm{Tr}(\boldsymbol{Q}^2)^2 \\ &= \frac{A}{2}Q_{\alpha\beta}Q_{\alpha\beta} - \frac{B}{3}Q_{\alpha\beta}Q_{\beta\gamma}Q_{\gamma\alpha} + \frac{C}{4}Q_{\alpha\beta}Q_{\alpha\beta}Q_{\gamma\delta}Q_{\gamma\delta}, \end{aligned} \tag{4}$$

where A, B, and C are some functions of pressure P and temperature T. Typical to Landau-type theories, this model equation of state predicts a phase transition near the temperature where A vanishes. It is often assumed that A has the form

$$A = A'(T - T^*).$$

The coefficients B and C are normally taken to be constants. In Section 7.1 we will show that the transition temperature itself is somewhat above T^*.

If the order parameter is slowly varying in space, the free energy will also contain gradients of the order parameter. As before, translational and rotational invariance restricts the combinations of derivatives of $\boldsymbol{Q}$. Taking into account the allowed combinations, the elastic free energy can be written as [13,14]

$$\begin{aligned} g_e =& \frac{L_1}{2}\frac{\partial Q_{ij}}{\partial x_k}\frac{\partial Q_{ij}}{\partial x_k} + \frac{L_2}{2}\frac{\partial Q_{ij}}{\partial x_j}\frac{\partial Q_{ik}}{\partial x_k} + \frac{L_3}{2}\frac{\partial Q_{ik}}{\partial x_j}\frac{\partial Q_{ij}}{\partial x_k} \\ &+ \frac{L_4}{2}e_{lik}Q_{lj}\frac{\partial Q_{ij}}{\partial x_k} + \frac{L_6}{2}Q_{lk}\frac{\partial Q_{ij}}{\partial x_l}\frac{\partial Q_{ij}}{\partial x_k}, \end{aligned} \tag{5}$$

where L_i are elastic constants. The first four terms are quadratic and the last term is cubic in the scalar order parameter. In fact, there are seven elastic terms of cubic order [15,16]. In Section 6 we will show that a uniaxial nematic has six independent bulk elastic constants. To model a nematic state with different elastic constants k_{11} and k_{33}, it is sufficient to include only the L_6 term.

The constants L_i are related to Frank-Oseen elastic constants by [13]

$$\begin{aligned} 6S^2L_1 &= k_{33} - k_{11} + 3k_{22}, \\ S^2L_2 &= k_{11} - k_{22} - k_{24}, \\ S^2L_3 &= k_{24}, \\ S^2L_4 &= 2t_0k_{22}, \\ 2S^3L_6 &= k_{33} - k_{11}, \end{aligned}$$

where S is the scalar nematic order parameter at which L_i are measured, t_0 is the chirality of the liquid crystal.

Typical values for a nematic compound 5CB are $A' = 0.044 \times 10^6\,\mathrm{J/m^3\,K}$, $B = 0.816 \times 10^6\,\mathrm{J/m^3}$, $C = 0.45 \times 10^6\,\mathrm{J/m^3}$, $L_1 = 6 \times 10^{-12}\,\mathrm{J/m}$, $L_2 = 12 \times 10^{-12}\,\mathrm{J/m}$, $T^* = 307\,\mathrm{K}$ [17]. The nematic-isotropic transition temperature for 5CB is $T_{NI} = 308.5\,\mathrm{K}$.

6. Frank-Oseen free energy

In an unstrained nematic, a uniform director orientation is the global minimum of its free energy. How much free energy does it take to deform this uniform director field? To answer this question, we can rewrite the Landau–de Gennes free energy in terms of the director $\boldsymbol{n}(\boldsymbol{r})$ by using the relation between the order tensor and the director, Eq. (2). An alternative approach is to consider curvature strains, or deformations of relative director orientations away from the equilibrium position. The restoring forces which arise to oppose these deformations are curvature stresses or torques. If the director

field varies slowly on the scale of intermolecular distances, the curvature stresses are proportional to the curvature strains. Equivalently, the free energy density is a quadratic function of the curvature strains.

In a local Cartesian coordinate system (x,y,z) with the z axis parallel to the director $\boldsymbol{n}$ (the x and y axes can be chosen arbitrarily because the liquid crystal is uniaxial) the six components of curvature are

$$\text{splay:} \quad s_1 = \frac{\partial n_x}{\partial x}, \quad s_2 = \frac{\partial n_y}{\partial y},$$
$$\text{twist:} \quad t_1 = -\frac{\partial n_y}{\partial x}, \quad t_2 = \frac{\partial n_x}{\partial y},$$
$$\text{bend:} \quad b_1 = \frac{\partial n_x}{\partial z}, \quad b_2 = \frac{\partial n_y}{\partial z}.$$

These deformation types are shown in Fig. 5.

The director deformation can be expanded in a Taylor series in powers of x, y, and z, which are measured from the local coordinate origin

$$n_x(\boldsymbol{r}) = s_1 x + t_2 y + b_1 z + \mathcal{O}(r^2),$$
$$n_y(\boldsymbol{r}) = -t_1 x + s_2 y + b_2 z + \mathcal{O}(r^2),$$
$$n_z(\boldsymbol{r}) = 1 + \mathcal{O}(r^2).$$

To obtain the free energy of a strained nematic, we now expand the elastic free energy up to the second order in strains,

$$g = \sum_{i=1}^{6} k_i a_i + \frac{1}{2}\sum_{i,j=1}^{6} k_{ij} a_i a_j, \tag{6}$$

where k_i and $k_{ij} = k_{ji}$ are the curvature elastic constants and $a_1 = s_1, a_2 = t_2, a_3 = b_1, a_4 = -t_1, a_5 = s_2, a_6 = b_2$.

Not all terms in this expansion are invariant with respect to the transformations which do not change the physical description of the liquid crystalline mesophase. In a uniaxial liquid crystal, the free energy density is invariant with respect to a rotation around the z axis. Considering a few special cases, such as rotations of $\frac{1}{2}\pi$ and $\frac{1}{4}\pi$ about z, we can show that there are only two independent moduli k_i, and that out of the thirty-six k_{ij}, only five are independent. The expression for the free energy density simplifies to

$$g = k_1(s_1 + s_2) + k_2(t_1 + t_2) + \frac{k_{11}}{2}(s_1 + s_2)^2 + \frac{k_{22}}{2}(t_1 + t_2)^2 + \frac{k_{33}}{2}\left(b_1^2 + b_2^2\right) + k_{12}(s_1 + s_2)(t_1 + t_2) - (k_{22} + k_{24})(s_1 s_2 + t_1 t_2).$$

The last term can be written as

$$s_1 s_2 + t_1 t_2 = \frac{\partial}{\partial x}\left(n_x \frac{\partial n_y}{\partial y}\right) - \frac{\partial}{\partial y}\left(n_x \frac{\partial n_y}{\partial x}\right).$$

It contributes only to the surface energy and can be omitted when studying bulk properties of liquid crystals.

In the presence of additional symmetries g can be simplified even further:

1. If the molecules are nonpolar or, if polar, are distributed with equal probability in the two directions, then the choice of the sign of $\boldsymbol{n}$ is arbitrary. We have chosen a right-handed coordinate system in which z is positive in the direction of $\boldsymbol{n}$. A reversal of $\boldsymbol{n}$ which retains the chirality of the coordinate system generates the transformation

   $$\boldsymbol{n} \to -\boldsymbol{n}, \quad x \to -x, \quad y \to -y, \quad z \to -z.$$

   Invariance of the free energy under this transformation requires

   $$k_1 = k_{12} = 0 \quad \text{(nonpolar)}.$$

   If $k_1 \neq 0$, the equilibrium state has finite splay.
2. In the absence of enantiomorphism, or chiral molecules which have different mirror images, g should be invariant with respect to reflections in the plane containing the z axis

   $$x \to x, \quad y \to -y, \quad z \to z.$$

   This introduces the constraints

   $$k_2 = k_{12} = 0 \quad \text{(mirror symmetry)}.$$

   If $k_2 \neq 0$ then the equilibrium state has finite twist and we are dealing with a cholesteric mesophase.

It is convenient to define

$$s_0 = -\frac{k_1}{k_{11}}, \quad t_0 = -\frac{k_2}{k_{22}}$$

and to add two constant terms to g, $\frac{1}{2}k_{11}s_0^2$ and $\frac{1}{2}k_{22}t_0^2$, so that it becomes evident that s_0 and t_0 are the splay and twist of the state which minimizes the free energy,

$$g = \frac{1}{2}k_{11}(s_1 + s_2 - s_0)^2 + \frac{1}{2}k_{22}(t_1 + t_2 - t_0)^2 + \frac{1}{2}k_{33}\left(b_1^2 + b_2^2\right) + k_{12}(s_1 + s_2)(t_1 + t_2).$$

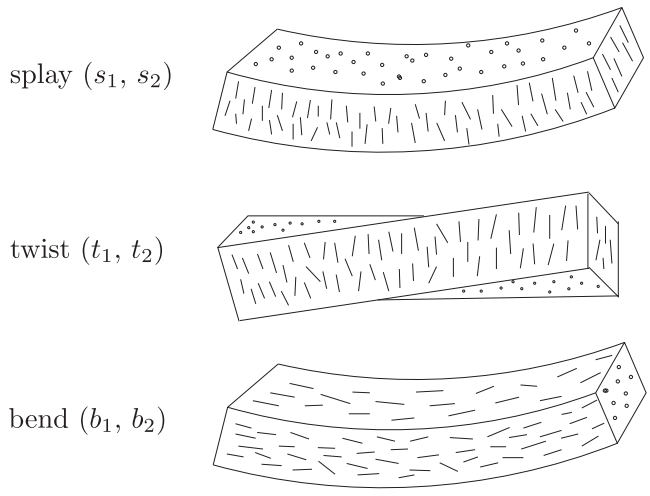

Fig. 5. The three distinct curvature strains of a uniaxial liquid crystal: splay, twist, and bend.

Here, s_0 vanishes in the absence of polarity, t_0 in the absence of enantiomorphy, and k_{12} vanishes unless both polarity and enantiomorphy occur together.

The free energy density can now be re-written in a vector notation. Substituting

$$s_1 + s_2 = \frac{\partial n_x}{\partial x} + \frac{\partial n_y}{\partial y} = \nabla \cdot \boldsymbol{n},$$
$$-(t_1 + t_2) = \frac{\partial n_y}{\partial x} - \frac{\partial n_x}{\partial y} = \boldsymbol{n} \cdot (\nabla \times \boldsymbol{n}),$$
$$b_1^2 + b_2^2 = \left(\frac{\partial n_x}{\partial z}\right)^2 + \left(\frac{\partial n_y}{\partial z}\right)^2 = (\boldsymbol{n} \times (\nabla \times \boldsymbol{n}))^2$$

into the expression for the free energy, we obtain the Frank-Oseen elastic free energy density for nematics and cholesterics

$$g = \frac{1}{2}k_{11}(\nabla \cdot \boldsymbol{n} - s_0)^2 + \frac{1}{2}k_{22}(\boldsymbol{n} \cdot (\nabla \times \boldsymbol{n}) + t_0)^2 + \frac{1}{2}k_{33}(\boldsymbol{n} \times (\nabla \times \boldsymbol{n}))^2 - k_{12}(\nabla \cdot \boldsymbol{n})(\boldsymbol{n} \cdot (\nabla \times \boldsymbol{n})). \quad (7)$$

It is sometimes useful to consider a nonpolar, nonenantiomorphic liquid crystal where bend, splay, and twist constants are equal (*one-constant* approximation). The free energy density for this model liquid crystal has a simple form,

$$g = \frac{1}{2}k\left[(\nabla \cdot \boldsymbol{n})^2 + (\nabla \times \boldsymbol{n})^2\right].$$

Minimizing the free energy $\int_V g dV$ with an additional constraint $\boldsymbol{n}^2 = 1$, we obtain the Euler-Lagrange equation for the director

$$-k_{11}\nabla(\nabla \cdot \boldsymbol{n}) + k_{22}[A(\nabla \times \boldsymbol{n}) + (\nabla \times (A\boldsymbol{n}))] + k_{33}[((\nabla \times \boldsymbol{n}) \times \boldsymbol{B}) + (\nabla \times (\boldsymbol{B} \times \boldsymbol{n}))] + \mu \boldsymbol{n} = 0,$$

where $A = \boldsymbol{n} \cdot (\nabla \times \boldsymbol{n})$, $\boldsymbol{B} = (\boldsymbol{n} \times (\nabla \times \boldsymbol{n}))$, μ is a Lagrange multiplier which can be determined from the condition $\boldsymbol{n}^2 = 1$.

7. Nematic-isotropic phase transition

In thermotropic liquid crystals, the isotropic to nematic phase transition takes place upon cooling. The densities of two mesophases are practically identical, and the transition has a weak first-order character. We will see that the ordered mesophases of thermotrops are stabilized by the enthalpic part of the free energy, while the orientational entropy favors the isotropic state. In lyotropic liquid crystals, the ordered and disordered mesophases have different densities, and the transition is driven by the competing rotational and translational entropies. After summarizing the results of the phenomenological Landau–de Gennes theory, we will discuss two molecular descriptions of the nematic-isotropic phase transition: the self-consistent mean-field approach of Maier and Saupe and the Onsager density functional theory.

7.1. Landau–de Gennes theory

In Section 4 we have shown that the tensorial order parameter of a uniaxial liquid crystal can be written as $Q_{\alpha\beta} = S\left(n_\alpha n_\beta - \frac{1}{3}\delta_{\alpha\beta}\right)$. Substituting this expression into Eq. (4), we can rewrite the excess free energy in terms of the scalar order parameter S,

$$g = \frac{1}{3}A'(T - T^*)S^2 - \frac{2}{27}BS^3 + \frac{1}{9}CS^4. \quad (8)$$

This dependence is shown in Fig. 6 for three different temperatures.

The value of S which minimizes this free energy is one of the solutions to the following equation,

$$AS - \frac{1}{3}BS^2 + \frac{2}{3}CS^3 = 0.$$

The two relevant solutions

$$S_I = 0,$$
$$S_N = (B/4C)[1 + (1 - 24\beta)^{1/2}],$$

where $\beta = AC/B^2$, correspond to the values of the order parameter in the isotropic and nematic mesophases, respectively.

At the transition temperature T_c the free energies of the isotropic and nematic mesophases are equal, which results in

$$\beta_c = \frac{1}{27}, \qquad T_c = T^* + \frac{1}{27}\frac{B^2}{A'C}, \qquad S_c = \frac{B}{3C}.$$

Above T_c the isotropic, below T_c the nematic state is stable.

The temperature T^* corresponds to the limit of metastability of the isotropic phase. It should be possible, in principle, to supercool the isotropic liquid to this temperature. At T^*, where the coefficient A in the free energy changes sign, $S = 0$ is no longer a local minimum of the free energy and the isotropic phase becomes unstable. Likewise, the nematic phase becomes unstable when $\beta > 1/24$. This determines a temperature $T^{**} = T^* + B^2/(24A'C)$ which sets the stability limit for the nematic mesophase upon heating.

The Landau–de Gennes theory predicts a discontinuous phase transition at a temperature T_c slightly above T^*. The source of this first-order phase transition is the odd-order powers of S in the expansion of the free energy density. These powers are present in the expansion because the sign of S has a clear physical meaning: it differentiates between the prolate and oblate molecular orderings.

7.2. Maier-Saupe theory

The Landau theory of the nematic-isotropic transition is entirely phenomenological: all molecular details are hidden in the material constants A, B, and C. Maier and Saupe have given the first microscopic

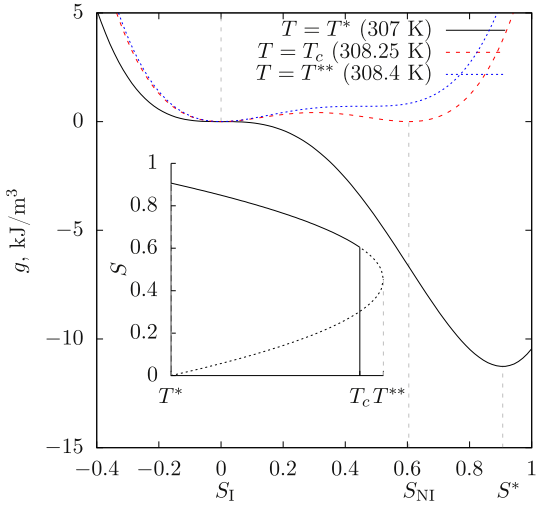

Fig. 6. Gibbs free energy density of a uniaxial nematic as a function of the scalar order parameter for the three temperatures, T^{**}, T_c, and T^* for 5CB. The inset shows the change of the order parameter with temperature.

model for the phase transition in a nematic liquid crystal [18,19]. The theory is based on three assumptions:

- Molecules interact via an orientation-dependent potential.
- The positions of the centers of mass of molecules are not affected by the orientation-dependent interaction.
- The mean field approximation.

In other words, a particular molecule interacts with an appropriately chosen external field. This field replaces the interaction of all the other molecules to an arbitrary molecule,

$$V(\boldsymbol{u},\boldsymbol{Q}) = -\frac{3}{2}vQ_{\alpha\beta}\left(u_\alpha u_\beta - \frac{1}{3}\delta_{\alpha\beta}\right), \tag{9}$$

where the molecular orientation is described by a unit vector $\boldsymbol{u}$.

The probability distribution function for the orientation of a molecule in the presence of this external field takes the form

$$f(\boldsymbol{u}) = \frac{1}{Z}\exp\left[-\frac{V(\boldsymbol{u},\boldsymbol{Q})}{k_BT}\right], \tag{10}$$

where $Z = \int d\boldsymbol{u}\exp(-V(\boldsymbol{u},\boldsymbol{Q})/k_BT)$ is the normalization factor, and $d\boldsymbol{u}$ indicates an integration over all orientations of $\boldsymbol{u}$. This distribution function is shown in Fig. 7 for several values of the scalar order parameter S.

The theory is made self-consistent by requiring the average value of $u_\alpha u_\beta - \frac{1}{3}\delta_{\alpha\beta}$ to be equal to $Q_{\alpha\beta}$,

$$Q_{\alpha\beta} = \int\left(u_\alpha u_\beta - \frac{1}{3}\delta_{\alpha\beta}\right)f(\boldsymbol{u})d\boldsymbol{u}.$$

For a uniaxial liquid crystal with the director oriented along the z axis we can define an angle θ between $\boldsymbol{u}$ and z. Using the relation between the tensorial and scalar order parameters discussed in Section 4, the zz component of this equation can be written as

$$S = \frac{2\pi}{Z}\int_0^\pi\left(\frac{3}{2}\cos^2\theta - \frac{1}{2}\right)\exp\left[-\frac{V(\theta,S)}{k_BT}\right]\sin\theta d\theta, \tag{11}$$

where $V(\theta,S) = -vS\left(\frac{3}{2}\cos^2\theta - \frac{1}{2}\right)$ and

$$Z = 2\pi\int_0^\pi\exp\left[-\frac{V(\theta,S)}{k_BT}\right]\sin\theta d\theta.$$

Eq. (11) has a trivial solution, $S = 0$, which corresponds to the isotropic phase. The second solution can be written in a parametric form after integrating by parts,

$$S = \frac{3}{4}\left[\frac{1}{xD(x)} - \frac{1}{x^2}\right] - \frac{1}{2}, \qquad \frac{k_BT}{v} = \frac{3}{2}\frac{S}{x^2},$$

where $D(x) = \exp(-x^2)\int_0^x\exp(y^2)dy$ is Dawson's integral. The dependence of S on T is shown in Fig. 8.

To analyze the stability of these solutions we need the expression for the free energy density of the system. The enthalpic part is given by the average interaction energy of a particle with the surrounding molecules,

$$\begin{aligned}U(T,S) &= \frac{1}{2}\langle V(\boldsymbol{u},\boldsymbol{Q})\rangle = -\frac{3}{4}vQ_{\alpha\beta}\int\left(u_\alpha u_\beta - \frac{1}{3}\delta_{\alpha\beta}\right)f(\boldsymbol{u})d\boldsymbol{u}\\ &= -\frac{3}{4}vQ_{\alpha\beta}Q_{\alpha\beta} = -\frac{3}{4}vS^2\left(\frac{1}{9}+\frac{1}{9}+\frac{4}{9}\right) = -\frac{1}{2}vS^2.\end{aligned}$$

Note that the prefactor 1/2 removes the double-counting of particle-particle interactions, which is an artifact of the mean-field approximation.

The entropy of the system with respect to its isotropic state can be calculated with the help of the Leibler–Kullback divergence,

$$\begin{aligned}D(T,S) &= -k_B\int\ln\frac{f(\boldsymbol{u})}{f_{iso}(\boldsymbol{u})}f(\boldsymbol{u})d\boldsymbol{u}\\ &= k_B\ln\left(\frac{Z}{4\pi}\right) + \frac{1}{T}\,V(\boldsymbol{u},\boldsymbol{Q}),\end{aligned}$$

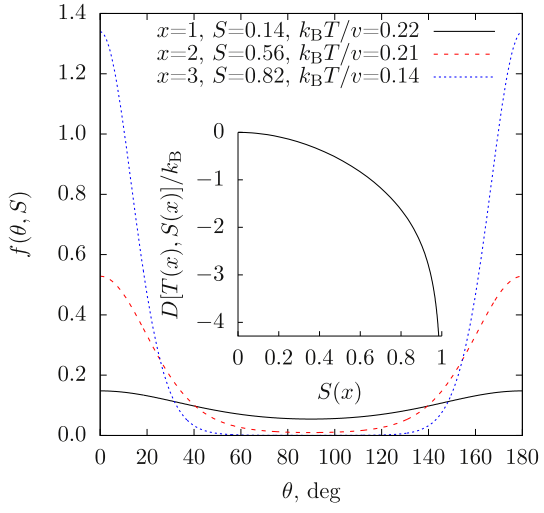

Fig. 7. Maier-Saupe theory: Distribution functions of molecular orientations for three different temperatures. At low temperatures two sharp peaks at 0 and 180° indicate that the mesophase is well aligned. The inset shows the entropy of the system relative to its isotropic phase. The entropy monotonically decreases with the increase of the scalar order parameter.

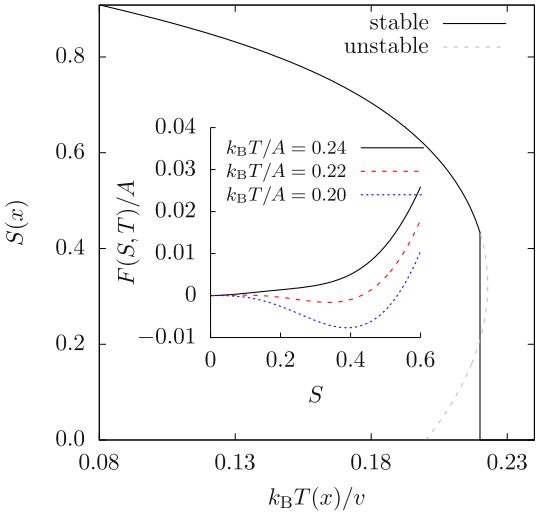

Fig. 8. Maier-Saupe theory: Dependence of the scalar order parameter on the dimensionless temperature. The nematic-isotropic transition takes place at $k_BT_c/v = 0.22$, $S_c = 0.43$. The inset shows corresponding free energy dependences on the order parameter S below, above, and at the transition.

where $f_{\rm iso}(\boldsymbol{u}) = \frac{1}{4\pi}$ is the distribution function of the isotropic phase. The dependence of this entropy on the scalar order parameter S is shown in the inset of Fig. 7.

The stable mesophase is given by the solution which minimizes the free energy per particle,

$$F(T,S) = U(T,S) - TD(T,S).$$

The dependence of this free energy on the order parameter S is shown in the inset of Fig. 8. The Maier-Saupe theory predicts a weak first-order phase transition at $k_{\rm B}T_c = 0.22v$ with the corresponding order parameter $S_c = 0.43$.

The Maier-Saupe theory can be re-formulated by postulating that the excess interaction energy is proportional to the square of the scalar order parameter, $U(T,S) = -\frac{1}{2}vS^2$ [20]. Using the variational calculus we can then show that the minimum of the free energy $F(T,S)$ is achieved for the distribution of molecular orientations given by Eq. (10).

7.3. Onsager theory

The Maier-Saupe theory is commonly applied to liquids which are only slightly compressible. Onsager [21] proposed a description which can be applied to dilute suspensions of particles where the change in free energy with density is relatively small. The Onsager theory predicts large changes in density at the transition, as is observed for such systems. Similar to Maier-Saupe, it is a molecular field theory, with the difference that the average energy is replaced by the orientation-dependent translational entropy.

As before, let us consider an ensemble of elongated particles interacting pairwise through some potential $\mathcal{V}(\mathbf{1},\mathbf{2})$ which now depends on both positions and orientations of molecules, $\mathbf{1} = (\boldsymbol{r}_1,\boldsymbol{u}_1)$. Onsager has shown how the Mayer cluster theory might be used to give an expansion for the equation of state of this system [21]. Onsager's expression for the Helmholtz free energy per particle is expressed in terms of the single-particle density, $\rho(\mathbf{1}) \equiv \rho(\boldsymbol{r}_1)f(\boldsymbol{r}_1,\boldsymbol{u}_1)$,

$$\beta F[\rho] = \int \rho(\mathbf{1})\left\{\ln\rho(\mathbf{1})\Lambda^3 - 1 - \beta\mu + \beta U(\mathbf{1})\right\} d(\mathbf{1}) - \frac{1}{2}\int f(\mathbf{1},\mathbf{2})\rho(\mathbf{1})\rho(\mathbf{2})d(\mathbf{1})d(\mathbf{2}). \quad (12)$$

Here $\beta = 1/k_{\rm B}T$, $\Lambda^2 = 2\pi\hbar^2\beta/m$ is the thermal de Broglie wavelength, μ is the chemical potential, $U(\mathbf{1})$ is the external potential energy, and $f(\mathbf{1},\mathbf{2}) = \exp\left[-\mathcal{V}(\mathbf{1},\mathbf{2})/k_{\rm B}T\right] - 1$ is the Mayer f-function.

The equilibrium single-particle density that minimizes this free energy is a solution of the Euler-Lagrange equation

$$\ln\rho(\mathbf{1})\Lambda^3 - \beta\mu + \beta U(\mathbf{1}) - \int f(\mathbf{1},\mathbf{2})\rho(\mathbf{2})d(\mathbf{2}) = 0, \quad (13)$$

obtained by the variation of the functional, Eq. (12).

For hard objects the integral of the Mayer f-function over spatial coordinates reduces to the excluded volume of these objects, since $\mathcal{V}(\mathbf{1},\mathbf{2}) = 0$ if they do not overlap and $\mathcal{V}(\mathbf{1},\mathbf{2}) = \infty$ if they overlap. For spherocylinders of length L and width D this excluded volume reads

$$E(\boldsymbol{u}_1,\boldsymbol{u}_2) = 2L^2D|\sin\gamma_{12}| + 2\pi LD^2 + \frac{4}{3}\pi D^3 \approx 2L^2D|\sin\gamma_{12}|,$$

where $\cos\gamma_{12} = \boldsymbol{u}_1\cdot\boldsymbol{u}_2$ and the approximate expression holds for $L \gg D$.

In a uniform nematic, $\rho(\boldsymbol{r}) = \text{const} \equiv \rho$, and the orientation-dependent part of the free energy reduces to

$$\beta F[f] = \int f(\boldsymbol{u})\ln f(\boldsymbol{u})d\boldsymbol{u} + \rho DL^2\int|\sin\gamma_{12}|f(\boldsymbol{u}_1)f(\boldsymbol{u}_2)d\boldsymbol{u}_1 d\boldsymbol{u}_2.$$

The first term in this expression is simply the rotational entropy of molecules, identical to the $D(T,S)$ in the Maier-Saupe theory, except that it is not measured with respect to the isotropic phase. Its dependence on the order parameter, which is shown in the inset of Fig. 9, is practically the same as the prediction of the Maier-Saupe theory. As anticipated, the rotational entropy decreases with the increase of the nematic order parameter. The second term is the excluded volume part of the translational entropy, which apparently depends on the mesophase ordering, since the excluded volume depends on the relative orientation of mesogens.

In the nematic state, γ_{12} are relatively small and the excluded volume gives rise to the translational entropy of the system which can be estimated as

$$\Delta S_{\rm tr} = -k_{\rm B}\ln\left(1 - V_{\rm excl}/V\right) \sim k_{\rm B}\rho L^2D,$$

where $\rho = N/V$ is the density of rods. However, there is also a decrease in the orientational entropy in the nematic state in comparison to the isotropic state

$$\Delta S_{\rm or} = k_{\rm B}\ln\Omega_N/\Omega_I \sim k_{\rm B},$$

where $\Omega_{I,N}$ is the number of orientational states in the isotropic and nematic mesophases, respectively. At the nematic-isotropic transition, these two contributions compensate each other, $\Delta S_{\rm or} \approx \Delta S_{\rm tr}$, predicting the critical density $\rho_c \sim 1/(L^2D)$, or a critical volume fraction $\phi_c = V_{\rm rods}/V \sim (NLD^2)/(NL^2D) = D/L$. Therefore, by increasing the length-to-breadth ratio we favor the formation of the nematic mesophase.

Eq. (13) can be solved numerically for any form of the second virial coefficient by expanding the density in Legendre polynomials. Direct minimization of the free energy functional is also possible and has the advantage that a well-chosen trial function can be used to

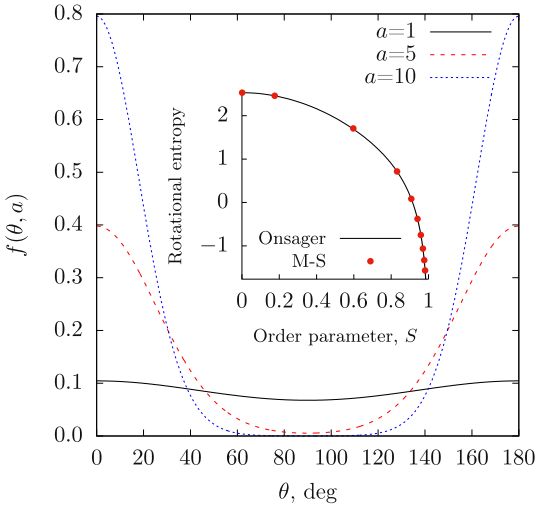

Fig. 9. Onsager theory: Distribution functions of molecular orientations for three different values of parameter a. The inset shows the entropy of the system with respect to its isotropic mesophase. Both Onsager and Maier-Saupe approaches are shown.

simplify the calculations. Onsager followed the latter approach and employed a one-parameter trial function for $f(\boldsymbol{u})$,

$$f(\boldsymbol{u}, a) = \frac{a\cosh(a\cos\theta)}{4\pi\sinh a},$$

where a is a variational parameter. This distribution is shown in Fig. 9 and is very similar to the distribution function of the Maier-Saupe theory. With the help of this ansatz, the dependence of the scalar order parameter S on the parameter a can be written as

$$S = 2\pi\int_0^\pi \left(\frac{3}{2}\cos^2\theta - \frac{1}{2}\right) f(\boldsymbol{u}, a)\sin\theta d\theta = 1 + \frac{3}{a^2} - \frac{3}{a\tanh a}.$$

The average of $\sin^2\gamma_{12} = \sin^2(\theta_1 - \theta_2) + \sin^2\theta_1\sin^2\theta_2\sin^2(\phi_1 - \phi_2)$ can be easily performed numerically after integrating over ϕ_1 and ϕ_2

$$\int_0^{2\pi} d\phi_1 \int_0^{2\pi} d\phi_2 \sin\gamma_{12} = 8\pi\sqrt{1+m}E\left(\frac{m}{1+m}\right),$$

where $E(m)$ is the complete elliptic integral of the second kind, and

$$m = \frac{\sin^2\theta_1\sin^2\theta_2}{\sin^2(\theta_1 - \theta_2) + \sin^2\theta_1\sin^2\theta_2}.$$

The numerical integration of the double integral over θ_1 and θ_2 provides the dependence of the translational entropy on the order parameter and is shown in Fig. 10, together with the rotational entropy. As expected, the two contributions compete: in an ordered system with $S \approx 1$ the rotational entropy is at its minimum, while the translational entropy is at its maximum, since the excluded volume is the smallest for $\gamma_{12} = 0$.

The inset of Fig. 10 illustrates the dependence of the free energy on the order parameter for three values of the dimensionless density, ρLD^2. If ρ is small, F has only one minimum at $a = 0$, which corresponds to the isotropic state. Above ρ_I, another minimum appears which corresponds to a nematic state. If ρ exceeds ρ_N, the minimum at $a = 0$ disappears, and there is only one minimum corresponding to the nematic state. Between ρ_I and ρ_N the free energy has two minima, and the thermodynamically favorable state is the one with

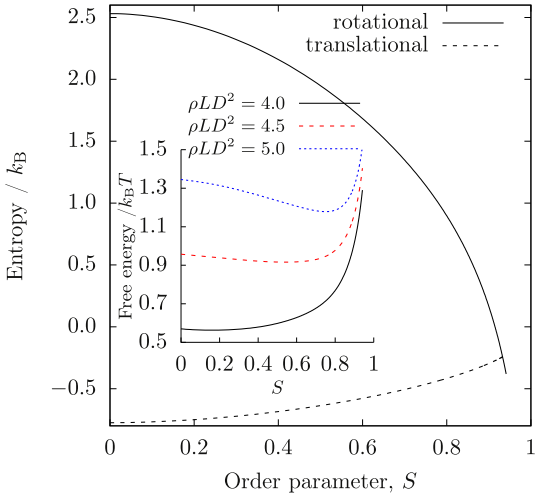

Fig. 10. Onsager theory: Translational and rotational entropies of the system as a function of the nematic order parameter. The inset shows the free energy of the system for three different dimensionless densities.

the lower free energy. It does not have to be an equilibrium state, because the free energy of the system can be lowered even more by a macroscopic phase separation. Indeed, if the system of density ρ and volume V separates into two phases with densities ρ_1 and ρ_2 and volumes V_1 and V_2, its total free energy changes to

$$F_{\text{total}} = V_1F_1 + V_2F_2 = \frac{\rho_2 - \rho}{\rho_2 - \rho_1}VF_1 + \frac{\rho - \rho_1}{\rho_2 - \rho_1}VF_2,$$

where we have used $\rho_1V_1 + \rho_2V_2 = \rho V$ and $V_1 + V_2 = V$.

This expression is simply a common tangent construction: it tells us that in a certain concentration range between ρ_A and ρ_B the free energy can be further minimized if the system is separated into an isotropic phase of concentration ρ_A and the nematic phase of concentration ρ_B. For $\rho < \rho_A$ the solution is isotropic and for $\rho > \rho_B$ it is nematic. An Onsager trial function predicts $\rho_A = 4.5/LD^2$, $\rho_B = 5.72/LD^2$, and $\rho_N = 5.1/LD^2$ [22]. A more accurate method gives $\rho_A = 4.19/LD^2$, $\rho_B = 5.37/LD^2$, and $\rho_N = 4.44/LD^2$ [23].

Note that the Onsager theory does not describe the bulk equation of state perfectly. The reason for this is the truncation of the virial expansion of the free energy at the leading, pairwise term: Onsager's results are applicable only for small volume fractions, $\phi = \rho\pi D^2L/4 \ll 1$. However, systematic improvements are possible and help to achieve a better agreement with the bulk equation of state [24–27].

8. Optical properties

In the uniaxial nematic, the dielectric susceptibility is a second-rank tensor with two eigenvalues, $\epsilon_\parallel$ and $\epsilon_\perp$, which are the susceptibilities per unit volume along and perpendicular to the director, respectively,

$$\epsilon_{ij} = \epsilon_\perp\delta_{ij} + \epsilon_a n_i n_j.$$

Correspondingly, it is possible to introduce ordinary and extraordinary refractive indexes,

$$n_e = \sqrt{\epsilon_\parallel}, \qquad n_o = \sqrt{\epsilon_\perp}, \qquad \Delta n = n_e - n_o.$$

For typical nematic liquid crystals, n_o is approximately 1.5 and Δn varies in the range between 0.05 and 0.5.

When a light beam enters a birefringent material, such as a nematic liquid crystal sample, it splits into ordinary and extraordinary rays. The two rays travel at different velocities and get out of phase. When these rays recombine after exiting the birefringent material, the polarization state of the light beam is a function of the phase difference. The length of the sample is therefore an important parameter: the phase shift accumulates as long as the light propagates in the birefringent material. Any polarization state can be produced with the right combination of the birefringence and length parameters.

Reflections at the layer boundaries and spatial variations of the optical axis complicate the description of light propagation in a liquid crystal. Here we use the 2 × 2-matrix formalism [28,29], though the 4 × 4 technique [30] is better suited for solving complicated reflection and transmission problems, especially on a computer.

In experimental setups, a liquid crystal sample is often placed between crossed polarizers. We adopt this geometry and assume that the first polarizer forms an angle α with respect to the director, as depicted in Fig. 11. The linearly polarized light after this polarizer,

$$\boldsymbol{E}_{\text{in}} = \begin{pmatrix} E_x \\ E_y \end{pmatrix} = \begin{pmatrix} E_0\cos\alpha \\ E_0\sin\alpha \end{pmatrix},$$

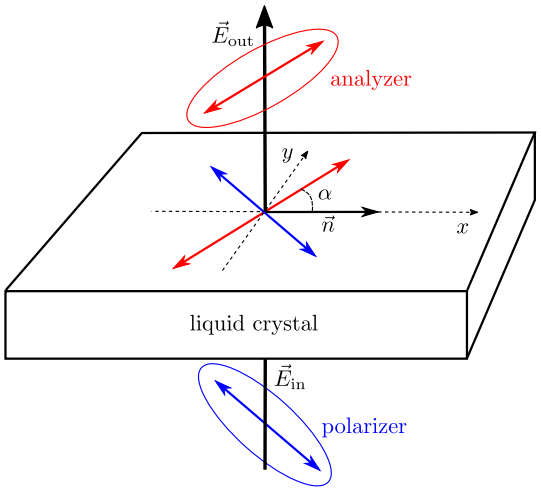

Fig. 11. Light traveling through a birefringent medium will take one of two paths, ordinary or extraordinary, perpendicular or parallel to the director, depending on its polarization.

becomes elliptically polarized after passing through the sample,

$$\boldsymbol{E}_{\text{lc}}(z) = \begin{pmatrix} E_x \exp(ik_e z) \\ E_y \exp(ik_o z) \end{pmatrix}.$$

Therefore, once the ray reaches the second polarizer, it has a component that can pass through it.

Using the Jones calculus for the optical polarizer

$$\hat{A} = \begin{pmatrix} \sin^2\alpha & -\cos\alpha\sin\alpha \\ -\cos\alpha\sin\alpha & \cos^2\alpha \end{pmatrix},$$

we obtain the light field,

$$\begin{aligned} \boldsymbol{E}_{\text{out}} &= \hat{A}\boldsymbol{E}_{\text{lc}}(z=d) \\ &= E_0 \sin(2\alpha)\sin\frac{\Delta k d}{2}\exp\frac{i(k_o+k_e)d}{2}\begin{pmatrix}\sin\alpha\\ \cos\alpha\end{pmatrix}, \end{aligned}$$

and the output light intensity behind the analyzer

$$|\boldsymbol{E}_{\text{out}}|^2 = E_0^2\sin^2(2\alpha)\sin^2\frac{\Delta k d}{2} = I_0\sin^2(2\alpha)\sin^2\frac{\pi\Delta n d}{\lambda}.$$

Hence, the phase shift determines the intensity of the transmitted light. For monochromatic light, the phase difference, $\pi\Delta nd/\lambda$, is determined by the thickness of the sample d and the birefringence of the material Δn. If the sample is very thin, the ordinary and extraordinary components do not get very far out of phase. If the phase difference equals 2π, the wave returns to its original polarization state and is blocked by the second polarizer. If the transmission axis of the first polarizer is parallel to either the ordinary or extraordinary directions, the light is not broken up into components, and no change in the polarization state occurs. In this case, $\alpha = 0$ or $\pi/2$, there is no transmitted component and the region appears dark.

In a typical liquid crystal, the birefringence varies through the sample. This means that some areas appear light and others appear dark, as in the image of the texture in Fig. 2 (a). The light and dark areas denote regions of differing director orientation, birefringence, and thickness. Birefringence can lead to multicolored images of liquid crystals in a polarized white light. Color patterns observed under the polarizing microscope can help to identify the textures of liquid crystal phases. To understand the origin of colors observed when liquid crystals are placed between crossed polarizers, it is helpful to consider the example of retarding plates. They are designed for a specific wavelength and thus will produce the desired results for a relatively narrow band of wavelengths around that particular value. For example, if a full-wave plate, designed for a wavelength λ, is placed between crossed polarizers at some arbitrary orientation and illuminated by white light, the wavelength λ will not be affected by the retarder and will be absorbed by the analyzer. However, all other wavelengths will experience some retardation and emerge from the full wave plate in a variety of polarization states. The components of this light which passed through the analyzer will then form the complementary to λ colors.

9. Response to external fields

The quintessential property of liquid crystals is that the director field is easily distorted by magnetic and electric fields as well as by substrates of the cell. This effect is due to a large anisotropy of their susceptibility tensors, which is again due to the anisotropic shape and susceptibility of molecules.

In the uniaxial case, the magnetic susceptibility is a second-rank tensor with two components $\chi_\parallel$ and $\chi_\perp$, which are the susceptibilities per unit volume along and perpendicular to the director. The susceptibility tensor can therefore be written as

$$\chi_{ij} = \chi_\perp\delta_{ij} + \chi_a n_i n_j,$$

where $\chi_a = \chi_\parallel - \chi_\perp$ is the anisotropy which is generally positive. The presence of a magnetic field $\boldsymbol{H}$ results in an extra term in the free energy,

$$g_m = -\frac{1}{2}\chi_{ij}H_iH_j = -\frac{1}{2}\chi_\perp H^2 - \frac{1}{2}\chi_a(\boldsymbol{n}\cdot\boldsymbol{H})^2.$$

The first term is usually omitted since it does not depend on the orientation of the director. The second term gives rise to a torque: if χ_a is positive the molecules will align parallel to the field.

The dielectric susceptibility of a liquid crystal is also anisotropic and has the same form as the magnetic susceptibility. In an electric field $\boldsymbol{E}$ there will be an additional free energy

$$g_e = -\frac{1}{8\pi}\epsilon_\perp E^2 - \frac{1}{8\pi}\epsilon_a(\boldsymbol{n}\cdot\boldsymbol{E})^2.$$

In principle, the same director reorientation can be achieved either with an electric or a magnetic field. In practice, the alignment of a liquid crystal by an electric field is complicated by the presence of conducting impurities, necessitating the use of alternating electric fields.

9.1. Fréedericksz transition in nematics

To illustrate the director response to the external magnetic or electric fields, let us consider a nematic liquid crystal oriented by two glass substrates, as shown in Fig. 12. The interaction between the nematic and the substrates is such that the director is aligned along the substrate normals. Experimental observations tell us that if a magnetic field is applied perpendicular to the director and its magnitude exceeds a certain critical value, the optical properties

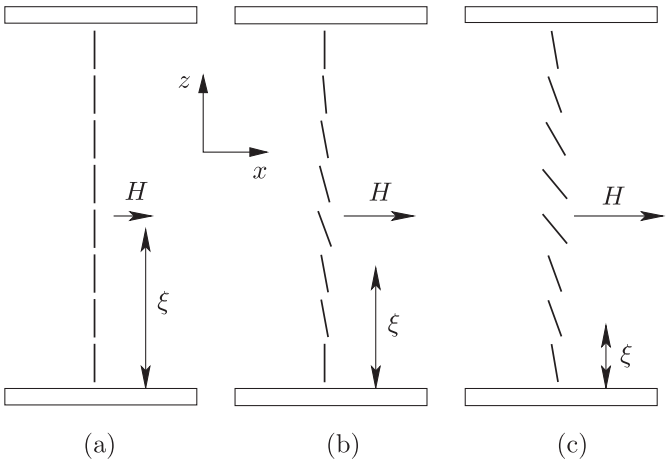

Fig. 12. The geometry of the Fréedericksz transition. The liquid crystal is perpendicular to the substrates, while the magnetic field is parallel to them. (a) Below a certain critical field H_c, the alignment is not affected. (b) Slightly above H_c, the deviation of the alignment sets in. (c) Once the field becomes stronger, the deviation increases.

of the system change abruptly. The reason is that both the magnetic field and the boundaries exert torques on the molecules. When the field exceeds certain critical value H_c, it becomes energetically favorable for the molecules in the bulk of the sample to turn in the direction of the field. This effect was first observed by Fréedericksz and Repiewa [31,32] and can be used to measure nematic elastic constants.

Let us assume that the z axis is perpendicular to the glass substrates and the field $\boldsymbol{H}$ is oriented along the x direction, so that the perturbation of the director field occurs only in this direction. The director components then read

$$n_x = \sin\theta, \qquad n_y = 0, \qquad n_z = \cos\theta,$$

where θ is the angle between the director and the z axis. The elastic energy per unit area, Eq. (7), takes the following form:

$$g = \frac{1}{2}\int_{-d/2}^{d/2} dz \left[\left(k_{11}\sin^2\theta + k_{33}\cos^2\theta\right)\left(\frac{\partial\theta}{\partial z}\right)^2 - \chi_a H^2 \sin^2\theta \right], \quad (14)$$

where d is the thickness of the sample.

In the undistorted case, $\theta = 0$, the field does not exert any torque on molecules, which are in a metastable equilibrium. To obtain an analytical solution above the critical field, we use the one-constant approximation, $k_{11} = k_{33} = k$, and introduce the magnetic coherence length $\xi = \sqrt{k/\chi_a H^2}$. The length ξ can be interpreted as a deformation length of the liquid crystal in the presence of an ordering field. It appears in many problems involving distortions produced by a magnetic field [11,12,33].

The free energy density, Eq. (14) then reads

$$g = \frac{1}{2}\frac{k}{\xi^2}\int_{-d/2}^{d/2} dz \left[\xi^2\left(\frac{\partial\theta}{\partial z}\right)^2 - \sin^2\theta \right].$$

Variation of this free energy leads to the Euler-Lagrange equation

$$\xi^2 \frac{\partial^2\theta}{\partial^2 z} + \sin\theta\cos\theta = 0. \quad (15)$$

The solution of this equation should satisfy the boundary conditions

$$\theta|_{z=-d/2,d/2} = 0.$$

For fields weaker than H_c only the trivial solution exists and there is no distortion on the nematic structure, $\theta = 0$. For larger fields, if the maximum distortion θ_m is small, $\sin\theta\cos\theta \approx \theta$, and $\theta = \theta_m \cos\frac{z}{\xi}$ is an approximate solution. The boundary conditions require that $d = \xi\pi$, or, equivalently,

$$H_c = \sqrt{\frac{k}{\chi_a}}\frac{\pi}{d}. \quad (16)$$

In fact, this relation holds even if $k_{11} \neq k_{33}$, in which case k should be substituted with k_{33}. Provided that χ_a is known, the measurement of H_c can be used to determine k_{33}.

The general solution to Eq. (15) can also be found in a closed form. The first integral of the Euler-Lagrange equation reads

$$\xi^2\left(\frac{\partial\theta}{\partial z}\right)^2 + \sin^2\theta = \sin^2\theta_m,$$

where the constant of integration has been identified by observing that $d\theta/dz = 0$ when θ is at its maximum value, θ_m. This maximum distortion lies halfway between the glass surfaces, at $z = 0$. Further integration gives

$$\frac{1}{2}d - z = \xi\int_0^\theta \frac{d\theta'}{\left(\sin^2\theta_m - \sin^2\theta'\right)^{1/2}} = \xi\csc\theta_m F(\csc\theta_m, \theta),$$

where F is the incomplete elliptic integral of the first kind, $\csc\theta = 1/\sin\theta$, and we have used the boundary condition $\theta = 0$ at $z = \pm\frac{1}{2}d$. The maximum distortion is found by substituting $z = 0$, $\theta = \theta_m$,

$$\frac{1}{2}d = \xi\csc\theta_m F(\csc\theta_m, \theta_m) = \xi K(\sin\theta_m),$$

where K is the complete elliptic integral of the first kind.

For fields just above H_c

$$\theta_m \sim 2\left(\frac{H}{H_c} - 1\right)^{1/2}.$$

The director profiles as well as exact and approximate dependencies of θ_m on H are shown in Fig. 13.

Fréedericksz's transition is easy to observe optically, since the average refractive index of the material changes when the magnetic field is applied. For the light beam polarized along the x axis in the geometry shown in Fig. 12, the local refractive index reads

$$n(z) = \frac{n_e n_o}{\left(n_e^2\sin^2\theta + n_o\cos^2\theta\right)^{1/2}},$$

and the average difference in the optical lengths of the ordinary and extraordinary waves is

$$\Delta n = \frac{1}{d}\int_{-d/2}^{d/2} dz\,[n(z) - n_o]. \quad (17)$$

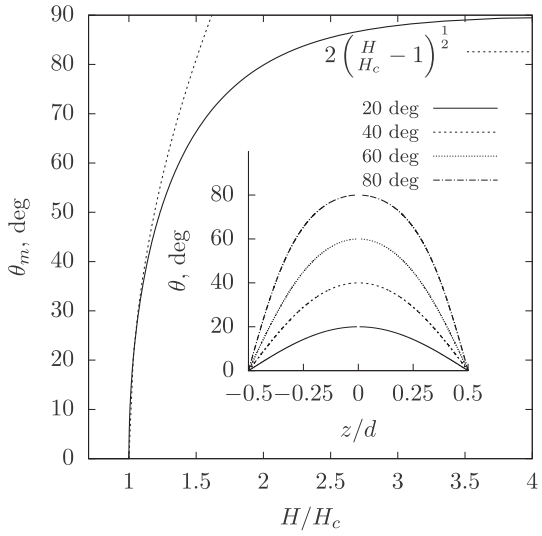

Fig. 13. Dependence of the maximum distortion angle in the middle of the cell, θ_m, on the external field H. The dashed line corresponds to the approximate solution. The inset shows the profiles of the director deviations in the cell for different field values.

Using Eq. (15), this can be rewritten as

$$\frac{\Delta n}{n_e} = 1 - \frac{2\xi}{d}\int_0^{\theta_m} \frac{d\theta}{(1+\nu\sin^2\theta)^{1/2}\left(\sin^2\theta_m - \sin^2\theta\right)^{1/2}} = 1 - \frac{2\xi}{d}\frac{1}{\left(1+\nu\sin^2\theta_m\right)^{1/2}} K\left(\frac{1+\nu}{\csc^2\theta_m + \nu}\right),$$

where $\nu = \left(n_e^2 - n_o^2\right)/n_o^2$. For small deformations the change in the refractive index is

$$\Delta n = n_e \nu \frac{H - H_c}{H_c} \tag{18}$$

and for large fields approaches $n_e - n_o$.

Fréedericksz's transition can be used to build the simplest liquid crystal display: since the optical properties of the cell depend on the reorientation of the director, the color of a pixel can be controlled by applying a voltage. A practical implementation of this idea will be discussed in Section 15.

10. Charge transport

Liquid crystalline compounds often contain π-conjugated segments, such as fused benzene and cyclopentadiene rings. Triphenylene, which is shown in Fig. 3, is a typical columnar liquid crystal with a conjugated core and solubilizing alkyl side chains. The delocalized π-orbitals of conjugated segments can easily donate or accept electrons, facilitating charge transfer reactions. Intermolecular charge transfer leads to charge transport, rendering these materials as organic semiconductors [34,35]. In their pristine state, however, organic semiconductors are insulators and become semiconducting only upon charge injection – from electrodes, by doping, or by photoexcitation.

Depending on the molecular arrangement and temperature, charge transport in liquid crystalline semiconductors can be band-like, disorder-limited, or thermally activated. Different transport regimes manifest themselves in different values and temperature dependencies of charge carrier mobility. The exponential increase of mobility with temperature, for example, indicates that transport is thermally activated. In this regime charges are localized and the transfer rate between these localized (diabatic) states can be approximated as [36,37]

$$k_{A\to B} = \frac{2\pi}{\hbar}\frac{J_{AB}^2}{\sqrt{4\pi\lambda kT}}\exp\left[-\frac{(\Delta U_{AB}-\lambda)^2}{4\lambda kT}\right].$$

This, so-called Marcus, rate depends on three microscopic parameters, namely the reorganization energy λ, the electronic coupling J_{AB}, and the driving force $\Delta U_{AB} = U_A - U_B$, all of which can be evaluated using quantum-chemical methods, classical polarizable force-fields, or quantum-classical hybrid methods [38].

The reorganization energy λ quantifies how much the geometry of the charge transfer complex and its environment adapts while the charge is transferred. The reorganization energy can be estimated based on four points on the diabatic potential energy surfaces,

$$\lambda_{A\to B} = U_{a,A} - U_{a,a} + U_{B,b} - U_{B,B},$$

where $U_{a,B}$ refers to the total energy of the molecule in state a and geometry B.

The electronic coupling J_{AB} is intimately related to the molecular overlap and therefore is very sensitive to relative positions and orientations of neighboring molecules. Correspondingly, charge carrier mobility varies from mesophase to mesophase. As a rule of thumb, more ordered mesophases have higher mobilities. Electronic coupling elements can be evaluated using semiempirical [39,40] or more accurate projection [41] methods.

The driving force ΔU_{AB} includes an internal contribution, namely the gas-phase electron affinity for electrons or ionization potential for holes. This contribution can vary from one molecular pair to another because of different energy levels for different types of molecules, or different conformers of the same molecule. The external contribution is due to the electrostatic and the induction interactions of a charge with the environment and is the most difficult to evaluate because the underlying interactions are long-ranged. To self-consistently account for both the electrostatic and the polarization effects, classical models are normally employed such as the polarizable force-fields [42,43].

In highly ordered systems with large electronic couplings the hopping picture breaks down. Charges delocalize and transport becomes limited by the dynamic disorder [44–46]. Furthermore, single crystals at low temperatures exhibit band-like charge transport with mobilities as high as tens $cm^2/V\,s$.

In line with mechanical properties, charge mobility in liquid crystals is often anisotropic. In columnar liquid crystals it is practically one-dimensional. The presence of a strong π-stacking direction inhibits other transport directions [47,48], since even a few defects can block charge drift along a column [49–51]. The lamellar arrangements of smectic liquid crystals, on the other hand, provide a two-dimensional transport network, ideally suited for field effect transistors. Semiconducting properties of liquid crystals have found their application in organic solar cells and field effect transistors [52].

11. Anchoring effects

The anchoring phenomenon is the tendency of liquid crystal molecules to orient themselves in a particular direction on the cell substrates. This orientation is called the easy orientation axis, $\boldsymbol{e}$. If the interaction of molecules with the substrate is strong, the director on this substrate always coincides with the easy orientation axis. This is termed strong anchoring. If this coupling is finite, the surface director deviates from the easy axis when, for example, an external field is applied. Orientation of the director perpendicularly to the substrate

is called homeotropic. Tangential, or planar, orientation implies that the director is parallel to the substrate.

Theoretical investigations of anchoring started with the early works on planar anchoring on grooved substrates [53]. On the phenomenological level, anchoring can be accounted for by adding a surface term to the total free energy of the system. The simplest form of the surface free energy was proposed by Rapini and Papoular [54],

$$F_s = -\frac{1}{2} W \int (\boldsymbol{n}\cdot\boldsymbol{e})^2 dS, \tag{19}$$

where the parameter W is the anchoring energy and $\boldsymbol{e}$ is a unit vector along the easy axis. These two parameters are critical for designing liquid crystal devices. A number of generalizations of the Rapini-Papoular potential were proposed [55], among them the generalization to the tensorial form,

$$F_s = -\frac{1}{2} W \mathrm{Tr}(\mathbf{Q}|_S - \mathbf{Q}_s)^2,$$

where $\mathbf{Q}_s$ is the value of the order tensor preferred by the surface and W is the anchoring energy. In case of uniaxial surface anchoring, $Q_{s,\alpha\beta} = S_s\left(e_\alpha e_\beta - \frac{1}{3}\delta_{\alpha\beta}\right)$.

Numerous experimental and theoretical methods were developed to measure the surface anchoring coefficient [56–62]. Available experimental data show that the length $\lambda = k_{33}/W$ is inversely proportional to the squared value of the bulk order parameter $\lambda \propto S^2$. Taking into account that the elastic constant k_{33} is proportional to S^2, we find $W \propto S^4$ for the anchoring parameter. Hence, anchoring strength can be efficiently controlled by temperature.

Most of the experimental methods measure surface director deviations in an external field and involve rather complicated optical setups. One of the simplest measurements of weak azimuthal anchoring strengths can be performed in a wedge cell with a twisted distribution of the director [60], as shown in Fig. 14. The easy axis on the reference substrate, where strong anchoring is assumed, makes an angle α with respect to the easy axis on the test substrate. The director orientation on the test substrate, ϕ_t, can be found from the condition $\sin\phi_t = \frac{\xi}{2}\sin 2(\alpha - \phi_t)$, where $\xi = Wd/k_{22}$, and d is the cell thickness. In a wedge cell d varies in the range ~0–50 μm. For $\alpha = \pi/4$ the explicit solution to this equation is

$$\sin\phi_t = \frac{1}{2}\left(\sqrt{2+\xi^{-2}} - \xi^{-1}\right).$$

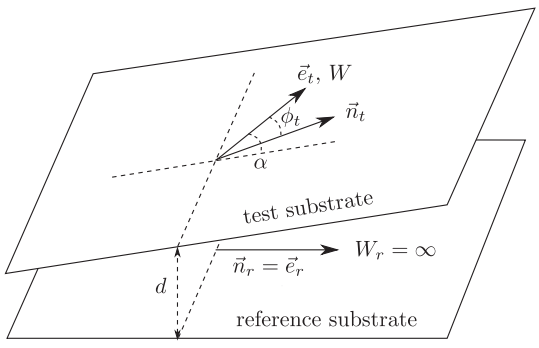

Fig. 14. Geometry of the wedge cell. The angle between the easy axis on the reference ($\boldsymbol{e}_r$) and the test ($\boldsymbol{e}_t$) substrates is α. The director $\boldsymbol{n}$ deviates from the test substrate easy axis by an angle ϕ_t.

If the polarizer is parallel to the easy axis on the reference substrate and the analyzer is oriented at an angle γ with respect to the polarizer, the light intensity behind the analyzer reads [63]

$$T = \frac{1}{2}\left(1 + T_c\cos 2\gamma + T_s \sin 2\gamma\right),$$
$$T_c = \left(\frac{u-1}{u+1}\sin^2\theta + \cos^2\theta\right)\cos 2\phi_t + \frac{\sin 2\theta}{\sqrt{u+1}}\sin 2\phi_t$$
$$T_s = \left(\frac{u-1}{u+1}\sin^2\theta + \cos^2\theta\right)\sin 2\phi_t - \frac{\sin 2\theta}{\sqrt{u+1}}\cos 2\phi_t$$
$$u = \left(\frac{\pi\Delta n d}{\lambda\phi_t}\right)^2, \qquad \theta = \phi_t\sqrt{u+1}.$$

The minimum of the transmission intensity is then given by

$$\gamma_A = \frac{1}{2}\arctan\frac{T_s}{T_c},$$

and is shown as a function of the cell thickness d in Fig. 15 for different values of anchoring strengths. This dependence can, of course, be measured in a single wedge cell. Though this method is only suitable for anchoring strengths of up to 10^{-2} erg/cm^2, its range and accuracy can be improved by using a magnetic field to control deviations of the director from the orientation of the easy axis [60].

12. Defects

Topological defects appear in physics as a consequence of a broken continuous symmetry [3]. They exist almost in every branch of physics: biological systems, superfluid helium, ferromagnets, crystalline solids, liquid crystals [64–67], quantum Hall fluids, and even optical fields [68], playing an important role in such phenomena as a response to external stresses and the nature and type of phase transitions. They even arise in certain cosmological models [69].

Liquid crystals are ideal materials for studying topological defects. Distortions yielding defects are easily produced through control of boundary conditions, surface geometries, and external fields. The resulting defects are easily imaged optically. The nematic liquid crystalline mesophase owes its name to the typical threadlike defect

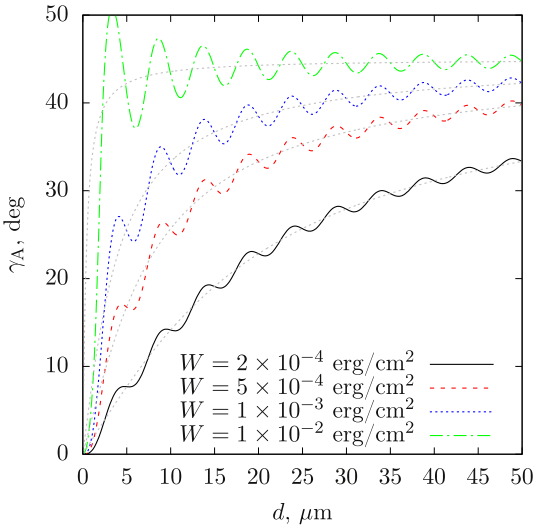

Fig. 15. Orientation of the analyzer which gives the minimum of the transmitted light intensity for different values of surface anchoring W. $\Delta n = 0.1$, $\lambda = 0.5$ μm, $k_{22} = 3.6\times10^{-7}$ erg/cm. Gray dotted lines show the director orientation at the substrate with finite anchoring (ϕ_t), thus illustrating deviations from the Mauguin regime.

which can be seen under a microscope in nematic and cholesteric phases [70].

First explanations of defects were given by Friedel [71], who suggested that these threads correspond to lines on which the director changes its direction discontinuously. In analogy with dislocations in crystals, Frank proposed calling them *disclinations*. To classify topological defects the homotopy theory can be employed [72]. In nematics, two types of stable topological defects in three dimensions exist: point defects, or *hedgehogs*, and line defects, or *disclinations*. Hedgehogs are characterized by an integer *topological charge q*, which specifies the number of times the unit sphere is wrapped by the director on any surface enclosing the defect core

$$q = \frac{1}{8\pi}\int dS_i \epsilon_{ijk}\boldsymbol{n}\cdot(\partial_j\boldsymbol{n}\times\partial_k\boldsymbol{n}),$$

where ∂_α denotes differentiation with respect to x_α, ϵ_{ijk} is the Levi-Civita symbol, and the integral is over any surface enclosing the defect core. For an order parameter with an O_3 (vector) symmetry, the order-parameter space is S^2, and hedgehogs can have positive or negative charges. Nematic inversion symmetry implies that positive and negative charges are equivalent.

The axial solutions of the Euler-Lagrange equations representing disclination lines are

$$\phi = m\theta + \phi_0,$$

where

$$n_x = \cos\phi, \qquad x = r\cos\theta,$$
$$n_y = \sin\phi, \qquad y = r\sin\theta,$$

and θ is the azimuthal angle (polar coordinates), m is a positive or negative integer or half-integer [2].

The director field around disclinations can be readily found from the condition

$$\frac{dy}{dx} = \tan(m\theta+\phi_0) \quad \text{or} \quad \frac{1}{r}\frac{dr}{d\theta} = \cot[(m-1)\theta+\phi_0],$$

which can be integrated in polar coordinates, yielding

$$\left(\frac{r}{r_0}\right)^{m-1} = \frac{\sin[(m-1)\theta+\phi_0]}{\sin[(m-1)\theta_0+\phi_0]}.$$

Examples of disclinations for several m are shown in Fig. 16.

The elastic energy per unit length associated with a disclination is $\pi K m^2 ln(R/r_0)$, where R is the size of the sample and r_0 is a lower cutoff radius, or the size of the disclination core [2]. Since the elastic energy is proportional to m^2, the formation of disclinations with large Frank indices m is energetically unfavorable.

Within the continuum Frank theory, disclinations are singular lines where the director gradients become infinite. This inevitably leads to a breakdown of the Frank-Oseen theory. The region near the singularity where this theory fails is called the disclination core. The phenomenological elastic theory predicts that a uniaxial nematic either melts or exhibits a complex biaxial structure in the core region [73]. Therefore, the core of the defect cannot be represented by the director field only, implying that biaxiality and variation of the order parameter should also be taken into account. For this reason, a more general theory based on the alignment tensor, Eq. (1), should be applied to provide the correct description of the core region [74–79].

A number of books and reviews are available on topological defects in liquid crystals and can be recommended for further reading [4,5,80].

13. Liquid crystal colloids

Long-range orientational ordering of molecules in liquid crystalline mesophases manifests itself in anisotropic mechanical properties of liquid crystals. If a liquid crystal is used as a host liquid in a colloidal suspension, this ordering gives rise to *long-range* anisotropic interactions between colloidal particles. Particle clustering, formation of superstructures, and even new phases are immediate consequences of these interactions.

To review the hierarchy of such interactions, we must first examine the director field around one particle suspended in a nematic host. The long-range interaction energy of two or more particles will follow directly from the dominant multipole moment of this director field, or its symmetry.

13.1. Defects around a colloidal particle

Two factors influence the director field around a colloidal particle: the particle size and the director orientation at its surface. A particle with a sufficiently strong homeotropic anchoring carries a topological charge of strength +1. If far away from the particle the director field is uniform, the total topological charge of the system is zero. To compensate the topological charge of the particle, an additional defect is created in the nematic. Depending on the particle size, two types of defects are observed. A *satellite* defect is a point defect with the topological charge of −1. Far from the particle, the director field of this particle-defect pair has dipolar symmetry, and two particles with such defects interact as a pair of dipoles. The other defect type is a −1/2 strength disclination ring that encircles the particle, or a *Saturn-ring* defect. This defect accompanies small colloids, has quadrupolar symmetry, and results in quadrupole-quadrupole interactions between colloids. Both types of defects are sketched in Fig. 17.

Experiments [81] as well as theories based on the Frank-Oseen elastic free energy [65,67,82,83] predict that the micron-sized particles stabilize the dipolar configuration. This defect can also acquire a director twist for large ratios of twist to splay elastic constants [82]. The Saturn-ring defect becomes a global minimum of the free energy once the particle size is reduced. The most stable position of the ring is in the equatorial plane, normal to the far-field director. By reducing the surface anchoring we can also stabilize a surface-ring director configuration [82,84].

13.2. Effective pair interactions

Experimenting with inverted nematic emulsions, Poulin et al. noticed that water droplets dispersed in a nematic solvent form linear chains that break upon the transition to the isotropic phase [85]. Droplet chaining is a clear manifestation of the long-range dipolar and short-range repulsive interactions [86]. Both dipolar and quadrupolar colloidal forces were measured directly using ferrofluid droplets in a magnetic field [87], magneto-optic tweezers [88–90], iron particles in a magnetic field [91], and dual-beam optical tweezers [92–94].

At large separations, nematic-mediated interactions between colloids can be directly related to a multipole expansion of the electrostatic interaction [65,95]. Indeed, in the one-constant approximation, the Frank-Oseen elastic free energy of small director deformations around the z-axis, $\boldsymbol{n}(\boldsymbol{r}) = (n_x, n_y, 1)$, can be written as

$$F \simeq \frac{k}{2}\int dr\left[(\nabla n_x)^2 + (\nabla n_y)^2\right].$$

Hence, far from the colloid the transverse director components, n_x and n_y, satisfy the Laplace equation. For a single particle, the solutions of this equation can be expanded into multipoles. Using the

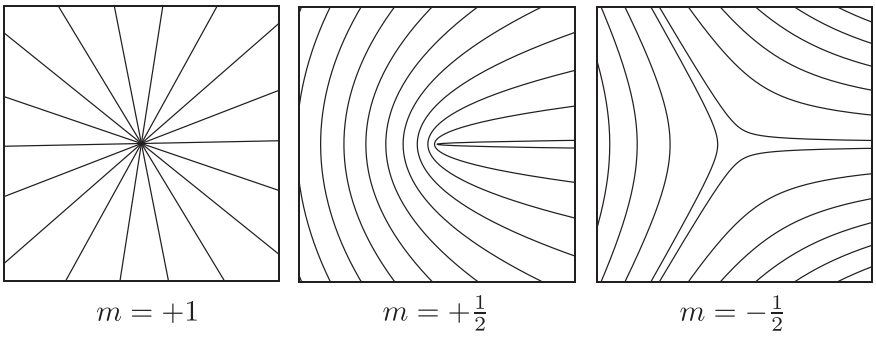

Fig. 16. Examples of axial disclinations in a nematic: with a topological charge, $m = +1$; the parabolic disclination, $m = +1/2$; and the hyperbolic disclination (topologically equivalent to the parabolic one), $m = -1/2$.

superposition principle, we can then obtain explicit expressions for the effective pair potential

$$V_{\text{dipl-dipl}} \propto \left(1 - 3\cos^2\theta\right) d^{-3},$$
$$V_{\text{quad-quad}} \propto \left(9 - 90\cos^2\theta + 105\cos^4\theta\right) d^{-5},$$
$$V_{\text{dipl-quad}} \propto \cos\theta(15\cos^2\theta - 9) d^{-4},$$

where d is the distance between the particles and θ is the angle between the far field orientation of the nematic director and the vector connecting the centers of the colloidal particles. These expressions can be generalized for particles of arbitrary shapes [96–98], weak anchoring at a particle surface [67], and different elastic constants [99].

The direct experimental measurements with optical tweezers confirmed the d^{-4} decay for two parallel ($\theta = 0$) dipoles [92-94,100]. However, for the antiparallel dipoles, the repulsive force decayed as $d^{-3.6}$ [94] and could be explained only by the direct integration of the stress tensor [101]. The d^{-5} decay of the dipole-quadrupole attraction ($\theta = \pi$) was also observed experimentally [102]. The quadrupolar, d^{-6}, tail was measured for colloidal particles with the tangential boundary conditions [88,103].

The electrostatic analogy of the linearized Frank-Oseen free energy in the one-elastic-constant approximation provides a valuable insight into assemblies of particles. Dipolar interactions promote long chains of colloids [100], while quadrupolar [104] or mixed [102,105] defects favor rhomboidal structures, in agreement with the angular dependences of interaction potentials.

At small interparticle separations, nonlinear effects become important: two Saturn rings can merge into one, repulsive forces can become attractive [106], etc. Many-body effects and nonlinearities require descriptions which go beyond the linearized theory and the superposition approximation. Numerical minimization of the Frank-Oseen [82,107,108] or Landau–de Gennes free energy [101,109-116], molecular dynamics [76-79,117], Monte Carlo [67], and classical density functional theory [118,119] are often used to study short-range interactions.

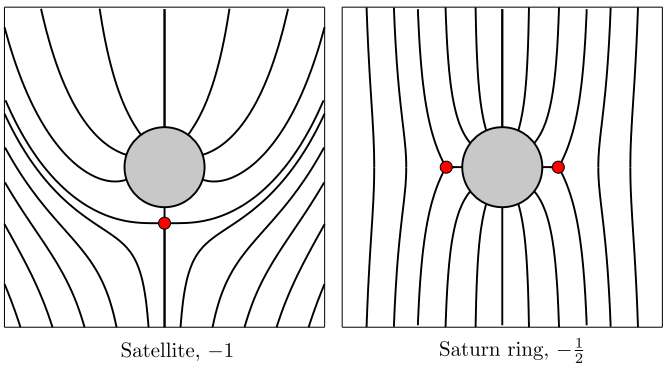

Fig. 17. Cross-sections of the director fields for the dipolar satellite and quadrupolar Saturn-ring defects accompanying a spherical colloid with homeotropic anchoring.

13.3. Colloids at a nematic-isotropic interface

Liquid-liquid interfaces provide an additional way of controlling colloidal assembly. In liquid crystals, a variety of ordered patterns can be observed at liquid-liquid interfaces [120–122]. The type and degree of ordering can be controlled by adding a molecular surfactant. For example, the addition of an anionic surfactant SDS to the liquid crystal 5CB triggers the formation of two-dimensional arrays with local hexagonal symmetry [122]. By doping the emulsion with a photosensitive amphiphilic dye we can control the nematic-air surface tension, the anchoring on the surface of droplets, and elastic constants of the host and hence manipulate the lattice constant of the two-dimensional hexagonal crystal formed by the glycerol droplets at the nematic-air interface [123]. By irradiating the emulsion with spatially-modulated light we can even obtain patterned two-dimensional colloidal crystals. More exotic situations include the coexistence of different two-dimensional assemblies of glycerol droplets at a nematic-air interface, which can be controlled by reorientation of elastic dipoles around each droplet [124].

Apart from controlling the assembly of particles at interfaces, it is also possible to use nematic-isotropic interfaces for ordering colloids into three-dimensional structures. For example, we can obtain cellular solids by dispersing colloidal particles in the isotropic phase of a liquid crystal and then quenching it below the NI transition temperature [125,126]. Colloidal particles, densely packed at thin interfaces between different nematic domains, form an open cellular structure with a characteristic domain size of 10–100 μm. The size of the domains can be controlled by changing the particle concentration. Due to the cellular morphology, such gel-like solids have a remarkably high elastic modulus, which varies linearly with the particle concentration [127].

When a colloidal particle is captured by a NI interface, it can be dragged by it. The speed of a moving NI interface controls the structural organization of colloidal particles. Periodic, stripe-like structures can be obtained, with the period depending on particle mass, size, and interface velocity [128–130]. The speed of the interface, the magnitude of the applied electric field, particle size, density and its dielectric properties control which particles can be moved and which are left behind. From a theoretical point of view, we can think of two origins of anisotropic interactions between particles pinned at the interface. First, the director deformations extend into the nematic

phase, i.e. in addition to the interfacial energy, the bulk elasticity contributes to the total free energy of the system. Second, the effective surface tension depends on the orientation of the director and hence varies along the interface due to the presence of colloidal particles.

Long-range elastic effects complicate our understanding of interparticle interactions at NI interfaces: expressions for the free energy or force-distance profiles can hardly be obtained analytically, especially for small separations, when many-body effects are important. For homeotropic anchoring, asymptotic analysis predicts that the elastic interaction is quadrupolar, repulsive, and decays with the distance as $(R/d)^{-5}$ [131,132]. Numerical calculations are also not straightforward. The interfacial width and the size of the defect core are normally much smaller than the size of a colloidal particle. Such disparate length-scales require solvers with adaptive meshes [133–135] and are reviewed in Ref. [106].

14. Computer simulation of liquid crystals

Computer simulations of liquid crystalline mesophases employ models of different complexity. Atomistic simulations, for example, use classical potentials to model inter- and intramolecular interactions. With their help we can link macroscopic properties of mesophases to their chemical composition [136]. To understand generic properties of liquid crystals, it is often sufficient to use coarse-grained models which lack chemical specificity but offer computational efficiency. Here we review one such model which is based on the anisotropic version of the Lennard–Jones potential, the Gay–Berne potential [8].

14.1. Molecular dynamics of non-spherical particles

Classical molecular dynamics is a numerical technique which solves the Newton's equations of motion for a system of molecules interacting via a given potential, v_{ij}. Since liquid crystal molecules have an elongated shape, the integration schemes should take into account orientational degrees of freedom, in addition to the translational ones. For a linear molecule with two equal and one zero principal moments of inertia, the angular velocity and the torque are both perpendicular to the molecular axis. If $\boldsymbol{e}_i$ is a unit vector along the molecular axis, then the torque on a molecule can be written as

$$\boldsymbol{\tau}_i = \boldsymbol{e}_i \times \boldsymbol{g}_i = \boldsymbol{e}_i \times \boldsymbol{g}_i^{\perp},$$

where $\boldsymbol{g}_i = -\nabla_{\boldsymbol{e}_i} v_{ij}$ is a "gorque" to be determined from the intermolecular forces. The vector $\boldsymbol{g}_i$ can always be replaced by its component perpendicular to the molecular axis, $\boldsymbol{g}_i^{\perp} = \boldsymbol{g}_i - (\boldsymbol{g}_i \cdot \boldsymbol{e}_i)\boldsymbol{e}_i$.

The equations for rotational motion can be written as two first-order differential equations [8],

$$\begin{aligned} \dot{\boldsymbol{e}}_i &= \boldsymbol{u}_i, \\ \dot{\boldsymbol{u}}_i &= \boldsymbol{g}_i^{\perp}/I_i + \lambda \boldsymbol{e}_i, \end{aligned} \tag{20}$$

where I_i is the moment of inertia, λ is a Lagrange multiplier which constrains the molecule length.

The equations of rotational motion and the Newton's equation of motion,

$$m_i \ddot{\boldsymbol{r}}_i = \boldsymbol{f}_i, \tag{21}$$

describe completely the dynamics of motion of a linear molecule. To solve these equations numerically, we have to adopt a proper discretization of them. Since the original equations of motion are time reversible, the discretized system has to be time reversible and conserve energy. Many discretizations fulfill these criteria: a quaternion algorithm [137], a rotation matrix algorithm, involving equations for Euler angles [8], a Gear predictor-corrector method [138]. The most widely used are the leap-frog and the velocity-Verlet algorithms [8]. The approach we describe here uses the leap-frog method [139].

To solve the equation for motion of the center of mass of molecules (Eq. (21)) using the leap-frog algorithm, we advance the velocities by half a step, using current accelerations $\boldsymbol{a}(t)$ and the previous velocities $\boldsymbol{v}\left(t - \frac{1}{2}\Delta t\right)$. Then the velocities and a new set of forces are calculated,

$$\begin{aligned} \boldsymbol{r}(t + \Delta t) &= \boldsymbol{r}(t) + \Delta t \boldsymbol{v}\left(t + \frac{1}{2}\Delta t\right), \\ \boldsymbol{v}\left(t + \frac{1}{2}\Delta t\right) &= \boldsymbol{v}\left(t - \frac{1}{2}\Delta t\right) + \Delta t \boldsymbol{a}(t). \end{aligned}$$

To evaluate the kinetic energy at time t the current velocities for time t can be calculated using

$$\boldsymbol{v}(t) = \frac{1}{2}\left[\boldsymbol{v}\left(t + \frac{1}{2}\Delta t\right) + \boldsymbol{v}\left(t - \frac{1}{2}\Delta t\right)\right].$$

Prior to solving the equation for rotational motion (Eq. (20)), a Lagrange multiplier λ has to be determined. By considering the advancement of coordinates over half a time step,

$$\boldsymbol{u}_i = \boldsymbol{u}_i\left(t - \frac{1}{2}\Delta t\right) + \frac{1}{2}\Delta t\left[\boldsymbol{g}_i^{\perp}(t)/I + \lambda(t)\boldsymbol{e}_i(t)\right].$$

and taking the scalar product of both sides with the vector $\boldsymbol{e}_i(t)$, we obtain

$$\lambda(t)\Delta t = -2\boldsymbol{u}_i\left(t - \frac{1}{2}\Delta t\right) \cdot \boldsymbol{e}_i(t).$$

We can now calculate $\dot{\boldsymbol{u}}_i(t)$ from Eq. (20) and then advance a full step in the integration algorithm,

$$\boldsymbol{u}_i\left(t + \frac{1}{2}\Delta t\right) = \boldsymbol{u}_i\left(t - \frac{1}{2}\Delta t\right) + \Delta t \dot{\boldsymbol{u}}_i(t).$$

The step is completed using

$$\boldsymbol{e}_i(t + \Delta t) = \boldsymbol{e}_i(t) + \Delta t \boldsymbol{u}_i\left(t + \frac{1}{2}\Delta t\right).$$

14.2. Forces and torques

To complete the problem, we have to derive forces and torques from the pairwise inter-particle potential $v_{ij}(\boldsymbol{r}_{ij}, \boldsymbol{e}_i, \boldsymbol{e}_j)$. If the centers of molecules are separated by a vector $\boldsymbol{r}_{ij}$ and the molecular axes are oriented along unit vectors $\boldsymbol{e}_i$ and $\boldsymbol{e}_j$, then the force on molecule i due to j reads

$$\boldsymbol{f}_{ij} = -\nabla_{\boldsymbol{r}_{ij}} v_{ij}.$$

Using the chain rule, we obtain

$$\boldsymbol{f}_{ij} = -\left(\frac{\partial v_{ij}}{\partial r_{ij}}\right)\nabla_{\boldsymbol{r}_{ij}} r_{ij} - \sum_{\alpha = i,j}\left(\frac{\partial v_{ij}}{\partial\left(\boldsymbol{n}_{ij} \cdot \boldsymbol{e}_\alpha\right)}\right)\nabla_{\boldsymbol{r}_{ij}}\left(\boldsymbol{n}_{ij} \cdot \boldsymbol{e}_\alpha\right),$$

where $\boldsymbol{n}_{ij} = \boldsymbol{r}_{ij}/r_{ij}$.

Taking into account that

$$\nabla_{\boldsymbol{r}_{ij}}\left(\boldsymbol{n}_{ij}\cdot\boldsymbol{e}_{\alpha}\right)=-\left(\boldsymbol{n}_{ij}\cdot\boldsymbol{e}_{\alpha}\right)\frac{\boldsymbol{r}_{ij}}{r_{ij}^{2}}+\frac{\boldsymbol{e}_{\alpha}}{r_{ij}},$$

where $\alpha = i,j$ we obtain

$$\boldsymbol{f}_{ij}=-\left(\frac{\partial v_{ij}}{\partial r_{ij}}\right)\boldsymbol{n}_{ij}-\sum_{\alpha=i,j}\left(\frac{\partial v_{ij}}{\partial\left(\boldsymbol{n}_{ij}\cdot\boldsymbol{e}_{\alpha}\right)}\right)\left(\frac{\boldsymbol{e}_{\alpha}}{r_{ij}}-\boldsymbol{r}_{ij}\frac{\left(\boldsymbol{n}_{ij}\cdot\boldsymbol{e}_{\alpha}\right)}{r_{ij}^{2}}\right).$$

To evaluate the torque on molecule i due to molecule j

$$\boldsymbol{\tau}_{ij}=-\boldsymbol{e}_{i}\times\nabla_{\boldsymbol{e}_{i}}v_{ij}$$

we again apply the chain rule, and obtain

$$\boldsymbol{\tau}_{ij}=-\boldsymbol{e}_{i}\times\left[\frac{\boldsymbol{r}_{ij}}{r_{ij}}\left(\frac{\partial v_{ij}}{\partial\left(\boldsymbol{n}_{ij}\cdot\boldsymbol{e}_{i}\right)}\right)+\boldsymbol{e}_{j}\left(\frac{\partial v_{ij}}{\partial\left(\boldsymbol{e}_{i}\cdot\boldsymbol{e}_{j}\right)}\right)\right].$$

We can see that $\boldsymbol{f}_{ij} = -\boldsymbol{f}_{ji}$ but $\boldsymbol{\tau}_{ij} \neq -\boldsymbol{\tau}_{ji}$.

Equations for forces and torques are the key ingredients of any molecular dynamics algorithm. To proceed further, we have to complement them with the pair interaction potential v_{ij}.

14.3. Gay–Berne intermolecular potential

The most widely used pair potential for coarse-grained liquid crystal simulations is the Gay–Berne potential, an extension of the Lennard–Jones potential to an anisotropic pair interaction [140,141],

$$v_{ij}=4\varepsilon\left(\rho^{-12}-\rho^{-6}\right),$$

where $\rho = [r_{ij} - \sigma + \sigma_s]/\sigma_s$.

The molecular shape parameter σ and the energy parameter ϵ depend on the molecular unit vectors $\boldsymbol{e}_i, \boldsymbol{e}_j$ as well as on the separation vector $\boldsymbol{n}_{ij}$ between the pair of molecules,

$$\left(\frac{\sigma_s}{\sigma}\right)^{2}=1-\frac{\chi}{2}\left[\xi(\chi,+1)+\xi(\chi,-1)\right],\quad\frac{\varepsilon}{\varepsilon_s}=(\varepsilon')^{\mu}(\varepsilon'')^{\nu},$$

where

$$\xi(\chi,s)=\frac{\left(\boldsymbol{e}_{i}\cdot\boldsymbol{n}_{ij}+s\boldsymbol{e}_{j}\cdot\boldsymbol{n}_{ij}\right)^{2}}{1+s\chi\boldsymbol{e}_{i}\cdot\boldsymbol{e}_{j}},$$

$$\varepsilon'=1-\frac{\chi'}{2}\left[\xi(\chi',+1)+\xi(\chi',-1)\right],$$

$$\varepsilon''=\left[1-\chi^{2}\left(\boldsymbol{e}_{i}\cdot\boldsymbol{e}_{j}\right)^{2}\right]^{-1/2}.$$

Here χ and χ' denote the anisotropy of the molecular shape and of the potential energy surface, respectively,

$$\chi=\frac{\kappa^{2}-1}{\kappa^{2}+1},\qquad\chi'=\frac{\kappa'^{1/\mu}-1}{\kappa'^{1/\mu}+1}.$$

The most important parameters of the potential are the anisotropy parameters κ and κ'. $\kappa = \sigma_e/\sigma_s$ is roughly the molecular elongation and the $\kappa' = \varepsilon_s/\varepsilon_e$ is the well-depth ratio for the side-by-side and end-to-end configurations. The Gay–Berne potential describes well generic properties of thermotropic liquid crystals [142]. Different variants of this potential are summarized in Table 1.

As an illustrative example, a simulation snapshot of two colloids immersed in a Gay–Berne liquid crystal is shown in Fig. 18. The mean interaction force between these colloids shows that the depletion forces dominate for small colloidal particles. The tangential component of the force can be used to resolve the elastic contribution to the total interaction and is different from the quadrupolar interaction predicted at large separations. The difference is due to the defect disposition and annihilation at small separations [117].

Table 1
Parameterizations of the Gay–Berne potential.

k	k'	μ	ν	Reference
3	5	2	1	[143,144]
3	5	1	3	[145]
3	5	1	2	[146]
3	–	0	0	Soft repulsive potential
4.4	20	1	1	[147]

14.4. The Monte Carlo technique

Since molecular dynamics becomes computationally inefficient at low densities, the Monte Carlo approach is the method of choice for simulating lyotropic liquid crystals. In Monte Carlo simulations, we begin with some configuration of molecular positions and orientations and then move and rotate molecules to generate trial configurations. When a trial configuration is generated, the difference in the potential energy $\Delta U = U_{\text{trial}} - U_{\text{old}}$ between the trial and old systems is calculated. If $\Delta U < 0$, the trial configuration is accepted and the process is repeated. If $\Delta U > 0$ the Boltzmann weight $\kappa = \exp(-\Delta U/k_{\text{B}}T)$ is compared to a random number $\eta \in (0 \ldots 1]$. If $\eta < \kappa$, the move is accepted, otherwise it is rejected. If ΔU is small, the Boltzmann factor is close to 1 and the acceptance of the trial configuration is highly probable. As ΔU increases, the trial moves become accepted with an ever lower probability. This means that big fluctuations in the energy are possible, but suppressed, leading to efficient phase space sampling. In practice, about half of the trial moves should be accepted [8]. In the Monte Carlo technique,

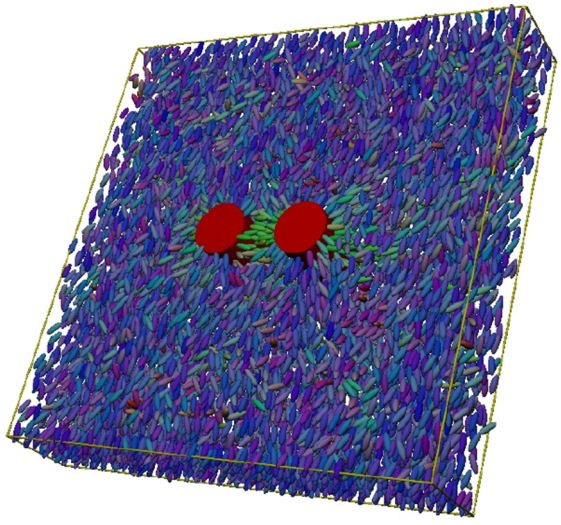

Fig. 18. Snapshot of molecular dynamics simulations of two long colloids immersed in a Gay–Berne liquid crystal. 8000 Gay–Berne particles, colloid radius $R/\sigma_0 = 3$, colloid separation $d/\sigma_0 = 10$. The color coding emphasizes particle orientations. Source: Adapted with permission from Phys. Rev. E 68, 051702. Copyright American Physical Society.

forces and torques are never calculated, only potential energies. As a consequence, neither real time nor real particle trajectories exist.

The Monte Carlo technique of a canonical (NVT) ensemble can be adapted to the constant pressure (NPT) ensemble. The volume changes can be implemented by scaling molecular positions. The probability function also changes according to the ensemble, $\kappa = \exp[-\{\Delta U + P\Delta V - Nk_BT\ln(1 - \Delta V/V)\}/k_BT]$. Volume changes are attempted far less often than molecular moves, to ensure that they are slow compared to molecular motion.

The Metropolis algorithm [148] described above generates configurations which are weighted to favor thermally populated states of the system. A number of important properties, such as free energies, require substantial sampling over higher-energy configurations. The non-Boltzmann sampling is more efficient in this case, with the old and trial states additionally weighted by a suitable function. This weighting encourages the system to explore regions of phase space which are not well sampled by the Metropolis method. The weighted averages are then corrected, giving desired ensemble averages. A particular example of non-Boltzmann sampling is the umbrella-sampling technique [8].

Monte Carlo and molecular dynamics simulations have been used to study various properties of liquid crystals, such as bulk elastic constants [149–153], viscosities [154,155], helical twisting power [156,157], parameters of the isotropic–nematic interface [158], confined geometries [61,62], and topological defects [77,159].

15. Applications

Discovered as early as 1888 [10], liquid crystals were treated as exotic substances for almost a century. In 1947, a modern transistor was invented. This invention triggered rapid miniaturization of electronic devices. The need for lightweight, power-efficient displays revitalized the research of electro-optical properties of liquid crystalline materials, and in 1970 Helfrich and Schadt filed a patent for a twisted nematic field effect. This technology soon grew into a multi-billion dollar industry [160]. Apart from displays, liquid crystals also found use in thin-film thermometers and switchable windows. Here, we explain working principles of these devices and link them to electro-optical properties of liquid crystals.

15.1. Liquid crystal displays

A single pixel of a twisted nematic display consists of two polarizing filters, two transparent electrodes, and a reflecting mirror, as depicted in Fig. 19. The liquid crystal itself is sandwiched between the transparent electrodes and is aligned by the substrates in such a way that there is a $\pi/2$ twist of the director in the cell. Before entering the liquid crystal, the incident light is polarized by the first polarizer. In the liquid crystal, light polarization follows the director distribution, which is often referred to as the Mauguin regime. As a result, its polarization is parallel to the second polarizer. The light ray is reflected back by the mirror. In this state, the pixel is reflecting light. With the application of a voltage, the twist of the director becomes distorted reorienting more and more along the field, perpendicular to the substrates. The Mauguin regime breaks down, the polarization of light no longer follows the twist of the director. The light beam is now blocked by the second polarizer and the pixel is absorbing light.

This type of cell can be found in old wristwatches, cell phones and calculator displays. Modern high resolution LCD panels of handheld and notebook computers use a white light source instead of a mirror, and the director in the cell is supertwisted rather than twisted, improving viewing angle characteristics of the display. A comprehensive overview of different types of liquid crystals displays is provided in Ref. [161].

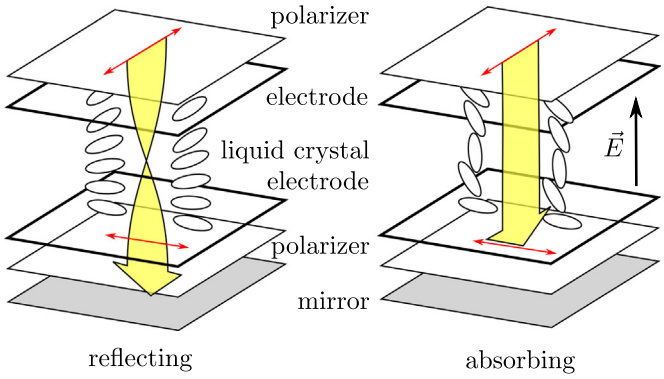

Fig. 19. Twisted nematic cell in its reflecting and absorbing states.

15.2. Liquid crystal thermometers

Chiral nematic or cholesteric liquid crystals reflect light with a wavelength equal to their pitch. As the pitch is sensitive to temperature variations, the color of the reflected light depends on temperature. It is therefore possible to determine temperature just by looking at the color of the thermometer. By mixing different compounds, devices for practically any temperature range can be built.

15.3. Polymer dispersed liquid crystals

Polymer dispersed liquid crystals consist of liquid crystal droplets dispersed in a solid polymer matrix, as shown in Fig. 20. The resulting material is a sort of “Swiss cheese” polymer with liquid crystal droplets filling in the holes. The tiny, only a few microns in diameter, droplets are responsible for the unique behavior of the material. The intensity of transmitted light can be varied by changing the orientation of the liquid crystal director in the droplets. In the off-state (no external field), the random orientation of the director in droplets leads to strong light scattering. The cell appears opaque. When the voltage is applied, the director aligns with the field, the refractive index of the liquid crystal matches the one of the matrix, and the cell becomes transparent.

Though liquid crystals are mostly known for their application in flat panel displays. their unique properties have been used in a number of other applications, such as organic electronics (Section 10), nanoparticle organization and liquid crystal colloids (Section 13), liquid crystal elastomer actuators, as well as chemical and biological sensors [10,162].

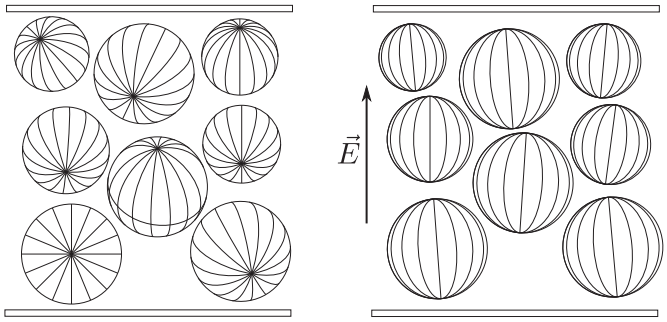

Fig. 20. In a typical polymer dispersed liquid crystal, droplets with different configurations and orientations scatter visible light. When an electric field is applied the molecules within the droplets align along the field and the material becomes transparent. In the following diagram, the director orientation is represented by the black lines on the droplet.

16. Supporting information

Python notebooks are provided for the following chapters:

- Fréedericksz transition, Section 9.1: Maximum distortion angle director profiles as a function of the applied magnetic field (freedericksz.ipynb).
- Defects, Section 12: Axial disclination lines in a nematic (defects.ipynb).
- Onsager theory, Section 7.3: Distribution functions, order parameter, rotational and translation entropies, free energy (onsager.ipynb).
- Maier-Saupe theory, Section 7.2: Distribution functions, rotational entropy, free energy, order parameter (maier_saupe.ipynb).
- Anchoring, Section 11: The analyzer position of the minimum transmission intensity as a function of the cell thickness (anchoring.ipynb).

Acknowledgments

I acknowledge Mykola Tasinkevych for his useful comments and Natacha Bouvier for proof-reading and continued support.

References

[1] P.G. de Gennes, J. Prost, The Physics of Liquid Crystals, 2nd edition ed., Clarendon Press. 1995.
[2] M.J. Stephen, J.P. Straley, Physics of liquid crystals, Rev. Mod. Phys. 46 (4) (1974) 617–704.
[3] P.M. Chaikin, T.C. Lubensky, Principles of Condensed Matter Physics, Cambridge University Press. 2000.
[4] O.D. Lavrentovich, M. Kleman, Cholesteric liquid crystals: defects and topology, Chirality in Liquid Crystals, Partially Ordered Systems, Springer, New York, NY, 2001, pp. 115–158.
[5] O.D. Lavrentovich, P. Pasini, C. Zannoni, S. Zumer (Eds.), Defects in Liquid Crystals: Computer Simulations, Theory and Experiments, Springer, Dordrecht; Boston., 2001,
[6] I.-C. Khoo, S.-T. Wu, Optics and Nonlinear Optics of Liquid Crystals, World Scientific. 1993.
[7] I. Dierking, Textures of Liquid Crystals, 1st edition ed., Wiley-VCH, Weinheim, 2003.
[8] M.P. Allen, D.J. Tildesley, Computer Simulation of Liquids, 2nd edition ed., Oxford University Press, Oxford, New York, 2017.
[9] E.G. Virga, Variational Theories for Liquid Crystals, 1st edition ed., Chapman and Hall/CRC, London, 1995.
[10] D. Dunmur, T. Sluckin, Soap, Science, and Flat-screen TVs: A History of Liquid Crystals, OUP Oxford. 2010.
[11] P. Oswald, P. Pieranski, Nematic and Cholesteric Liquid Crystals: Concepts and Physical Properties Illustrated by Experiments, CRC Press. 2005.(google-Books-ID: 4W3YXuUFAGMC).
[12] P. Oswald, P. Pieranski, Smectic and Columnar Liquid Crystals: Concepts and Physical Properties Illustrated by Experiments, CRC Press. 2005.(google-Books-ID: f4Q1m9cLEaEC).
[13] H. Mori, J.E.u.g.e.n.e.C. Gartland, J.R. Kelly, P.J. Bos, Multidimensional director modeling using the Q tensor representation in a liquid crystal cell and its application to the π cell with patterned electrodes, Jpn. J. Appl. Phys. 38 (1R) (1999) 135.
[14] N.J. Mottram, C.J.P. Newton, Introduction to Q-tensor theory, 2014. arXiv:1409.3542 [cond-mat]ArXiv: 1409.3542.
[15] K. Schiele, S. Trimper, On the elastic constants of a nematic liquid crystal, Phys. Status Solidi B 118 (1) (1983) 267–274.
[16] D.W. Berreman, S. Meiboom, Tensor representation of Oseen-Frank strain energy in uniaxial cholesterics, Phys. Rev. A 30 (4) (1984) 1955–1959.
[17] H.J. Coles, Laser and electric field induced birefringence studies on the cyanobiphenyl homologues, Mol. Cryst. Liq. Cryst. 49 (3) (1978) 67–74.
[18] W. Maier, A. Saupe, Eine einfache molekulare Theorie des nematischen kristallinflüssigen Zustandes, Z. Naturforsch. A 13 (7) (2014) 564–566. (In German.).
[19] W. Maier, A. Saupe, Eine einfache molekular-statistische Theorie der nematischen kristallinflüssigen Phase. Teil I1., Z. Naturforsch. A 14 (10) (2014) 882–889. (In German.).
[20] R.A.L. Jones, Soft Condensed Matter, OUP Oxford. 2002.
[21] L. Onsager, The effects of shape on the interaction of colloidal particles, Ann. N. Y. Acad. Sci. 51 (4) (1949) 627–659.
[22] M. Doi, S.F. Edwards, The Theory of Polymer Dynamics, Clarendon Press. 1988.
[23] G. Lasher, Nematic ordering of hard rods derived from a scaled particle treatment, J. Chem. Phys. 53 (11) (1970) 4141–4146.
[24] P.J. Camp, C.P. Mason, M.P. Allen, A.A. Khare, D.A. Kofke, The isotropic–nematic phase transition in uniaxial hard ellipsoid fluids: coexistence data and the approach to the Onsager limit, J. Chem. Phys. 105 (7) (1996) 2837–2849.
[25] J.D. Parsons, Nematic ordering in a system of rods, Phys. Rev. A 19 (3) (1979) 1225–1230.
[26] S.-D. Lee, A numerical investigation of nematic ordering based on a simple hard-rod model, J. Chem. Phys. 87 (8) (1987) 4972–4974.
[27] S.-D. Lee, The Onsager-type theory for nematic ordering of finite-length hard ellipsoids, J. Chem. Phys. 89 (11) (1988) 7036–7037.
[28] R.C. Jones, A new calculus for the treatment of optical systems. I. Description and discussion of the calculus, JOSA 31 (7) (1941) 488–493.
[29] S. Teitler, B.W. Henvis, Refraction in stratified, anisotropic media, JOSA 60 (6) (1970) 830–834.
[30] D.W. Berreman, Optics in stratified and anisotropic media: 4 × 4-matrix formulation, JOSA 62 (4) (1972) 502–510.
[31] V. Fréedericksz, A. Repiewa, Theoretisches und Experimentelles zur Frage nach der Natur der anisotropen Flüssigkeiten, Z. Phys. 42 (7) (1927) 532–546. (In German.).
[32] V. Fréedericksz, V. Zolina, Forces causing the orientation of an anisotropic liquid, Trans. Faraday Soc. 29 (140) (1933) 919–930.
[33] L.M. Blinov, V.G. Chigrinov, Electrooptic Effects in Liquid Crystal Materials, Springer Science & Business Media. 1996.(google-Books-ID: R1nafowHQikC).
[34] S. Kusabayashi, M.M. Labes, Conductivity in liquid crystals, Mol. Cryst. 7 (1) (1969) 395–405.
[35] J.-I. Hanna, Charge carrier transport in liquid crystalline semiconductors, Liquid Crystalline Semiconductors, Springer Series in Materials Science, Springer, Dordrecht, 2013, pp. 39–64. https://doi.org/10.1007/978-90-481-2873-0_2.
[36] R.A. Marcus, Electron transfer reactions in chemistry. Theory and experiment, Rev. Mod. Phys. 65 (3) (1993) 599–610.
[37] V. May, O. Kühn, Charge and Energy Transfer Dynamics in Molecular Systems, 3rd edition ed., Wiley-VCH. 2011.(bibtex: may_charge_2011).
[38] V. Rühle, A. Lukyanov, F. May, M. Schrader, T. Vehoff, J. Kirkpatrick, B. Baumeier, D. Andrienko, Microscopic simulations of charge transport in disordered organic semiconductors, J. Chem. Theory Comput. 7 (10) (2011) 3335–3345.
[39] J.L. Brédas, J.P. Calbert, D.A.d.S. Filho, J. Cornil, Organic semiconductors: a theoretical characterization of the basic parameters governing charge transport, Proc. Natl. Acad. Sci. U. S. A. 99 (9) (2002) 5804–5809.
[40] J. Kirkpatrick, An approximate method for calculating transfer integrals based on the ZINDO Hamiltonian, Int. J. Quantum Chem. 108 (1) (2008) 51–56.
[41] B. Baumeier, J. Kirkpatrick, D. Andrienko, Density-functional based determination of intermolecular charge transfer properties for large-scale morphologies, Phys. Chem. Chem. Phys. 12 (36) (2010) 11103.
[42] C. Poelking, D. Andrienko, Long-range embedding of molecular ions and excitations in a polarizable molecular environment, J. Chem. Theory Comput. 12 (9) (2016) 4516–4523.
[43] G. D'Avino, L. Muccioli, F. Castet, C. Poelking, D. Andrienko, Z.G. Soos, Jérôme Cornil, D. Beljonne, Electrostatic phenomena in organic semiconductors: fundamentals and implications for photovoltaics, J. Phys. Condens. Matter 28 (43) (2016) 433002.
[44] A. Troisi, Charge transport in high mobility molecular semiconductors: classical models and new theories, Chem. Soc. Rev. 40 (5) (2011) 2347.
[45] T. Vehoff, Y.S. Chung, K. Johnston, A. Troisi, D.Y. Yoon, D. Andrienko, Charge transport in self-assembled semiconducting organic layers: role of dynamic and static disorder, J. Phys. Chem. C 114 (23) (2010) 10592–10597.
[46] S. Fratini, D. Mayou, S. Ciuchi, The transient localization scenario for charge transport in crystalline organic materials, Adv. Funct. Mater. 26 (14) (2016) 2292–2315.
[47] M. Schrader, C. Körner, C. Elschner, D. Andrienko, Charge transport in amorphous and smectic mesophases of dicyanovinyl-substituted oligothiophenes, J. Mater. Chem. 22 (41) (2012) 22258–22264.
[48] M. Schrader, R. Fitzner, M. Hein, C. Elschner, B. Baumeier, K. Leo, M. Riede, P. Bäuerle, D. Andrienko, Comparative study of microscopic charge dynamics in crystalline acceptor-substituted oligothiophenes, J. Am. Chem. Soc. 134 (13) (2012) 6052–6056.
[49] J. Kirkpatrick, V. Marcon, J. Nelson, K. Kremer, D. Andrienko, Charge mobility of discotic mesophases: a multiscale quantum and classical study, Phys. Rev. Lett. 98 (22) (2007) 227402.
[50] X. Feng, V. Marcon, W. Pisula, M.R. Hansen, J. Kirkpatrick, F. Grozema, D. Andrienko, K. Kremer, K. Müllen, Towards high charge-carrier mobilities by rational design of the shape and periphery of discotics, Nat. Mater. 8 (5) (2009) 421–426.
[51] F. May, V. Marcon, M.R. Hansen, F. Grozema, D. Andrienko, Relationship between supramolecular assembly and charge-carrier mobility in perylenediimide derivatives: the impact of side chains, J. Mater. Chem. 21 (26) (2011) 9538–9545.
[52] W. Pisula, X. Feng, K. Müllen, Organic electronics: tuning the columnar organization of discotic polycyclic aromatic hydrocarbons (Adv. Mater. 33/2010), Adv. Mater. 22 (33). (2010)(n/a–n/a).
[53] D.W. Berreman, Solid surface shape and the alignment of an adjacent nematic liquid crystal, Phys. Rev. Lett. 28 (26) (1972) 1683–1686.
[54] A. Rapini, M. Papoular, Distorsion D'une Lamelle Nématique Sous Champ Magnétique Conditions D'ancrage Aux Parois, J. Phys. Colloq. 30 (C4). (1969)C4–54–C4–56. (In French.).

[55] S.V. Shiyanovskii, A. Glushchenko, Y. Reznikov, O.D. Lavrentovich, J.L. West, Tensor and complex anchoring in liquid crystals, Phys. Rev. E 62 (2) (2000) R1477–R1480.
[56] D. Subacius, V.M. Pergamenshchik, O.D. Lavrentovich, Measurement of polar anchoring coefficient for nematic cell with high pretilt angle, Appl. Phys. Lett. 67 (2) (1995) 214–216.
[57] H. Yokoyama, H.A. van Sprang, A novel method for determining the anchoring energy function at a nematic liquid crystal-wall interface from director distortions at high fields, J. Appl. Phys. 57 (10) (1985) 4520–4526.
[58] Y.A. Nastishin, R.D. Polak, S.V. Shiyanovskii, V.H. Bodnar, O.D. Lavrentovich, Nematic polar anchoring strength measured by electric field techniques, J. Appl. Phys. 86 (8) (1999) 4199–4213.
[59] D.-F. Gu, S. Uran, C. Rosenblatt, A simple and reliable method for measuring the liquid crystal anchoring strength coefficient, Liq. Cryst. 19 (4) (1995) 427–431.
[60] D. Andrienko, A. Dyadyusha, A. Iljin, Y. Kurioz, Y. Reznikov, Measurement of azimuthal anchoring energy of nematic liquid crystal on photoaligning polymer surface, Molecular Crystals and Liquid Crystals Science and Technology. Section A, Mol. Cryst. Liq. Cryst. 321 (1) (1998) 271–281.
[61] M.P. Allen, Molecular simulation and theory of liquid crystal surface anchoring, Mol. Phys. 96 (1999) 1391–1397.
[62] D. Andrienko, G. Germano, M.P. Allen, Liquid crystal director fluctuations and surface anchoring by molecular simulation, Phys. Rev. E 62 (5) (2000) 6688–6693.
[63] T. Akahane, H. Kaneko, M. Kimura, Novel method of measuring surface torsional anchoring strength of nematic liquid crystals, Jpn. J. Appl. Phys. 35 (8R) (1996) 4434.
[64] E.C.J. Gartland, P. Palffy-muhoray, R.S. Varga, Numerical minimization of the Landau-de Gennes free energy: defects in cylindrical capillaries, Mol. Cryst. Liq. Cryst. 199 (1) (1991) 429–452.
[65] T.C. Lubensky, D. Pettey, N. Currier, H. Stark, Topological defects and interactions in nematic emulsions, Phys. Rev. E 57 (1) (1998) 610–625.
[66] O. Mondain-Monval, J.C. Dedieu, T. Gulik-Krzywicki, P. Poulin, Weak surface energy in nematic dispersions: Saturn ring defects and quadrupolar interactions, Eur. Phys. J. B 12 (2) (1999) 167–170.
[67] R.W. Ruhwandl, E.M. Terentjev, Monte Carlo simulation of topological defects in the nematic liquid crystal matrix around a spherical colloid particle, Phys. Rev. E 56 (5) (1997) 5561–5565.
[68] M.S. Soskin, M.V. Vasnetsov, Nonlinear singular optics, Pure Appl. Opt. J. Eur. Opt. Soc Part A 7 (2) (1998) 301.
[69] B. Yurke, A.N. Pargellis, N. Turok, Coarsening dynamics in nematic liquid crystals, Mol. Cryst. Liq. Cryst. Sci. Technol. Sect. A Mol. Cryst. Liq. Cryst. 222 (1) (1992) 195–203.
[70] D. Demus, L. Richter, Textures of Liquid Crystals, Wiley-VCH, Weinheim, 1978.
[71] G. Friedel, Les états mésomorphes de la matière, Ann. Phys. 9 (18) (1922) 273–474. (In French.).
[72] N.D. Mermin, The topological theory of defects in ordered media, Rev. Mod. Phys. 51 (3) (1979) 591–648.
[73] P. Biscari, Intrinsically biaxial systems: a variational theory for elastomers, Molecular Crystals and Liquid Crystals Science and Technology. Section A, Mol. Cryst. Liq. Cryst. 299 (1) (1997) 235–243.
[74] N. Schopohl, T.J. Sluckin, Defect core structure in nematic liquid crystals, Phys. Rev. Lett. 59 (22) (1987) 2582–2584.
[75] A. Sonnet, A. Kilian, S. Hess, Alignment tensor versus director: description of defects in nematic liquid crystals, Phys. Rev. E 52 (1) (1995) 718–722.
[76] J.L. Billeter, R.A. Pelcovits, Defect configurations and dynamical behavior in a Gay-Berne nematic emulsion, Phys. Rev. E 62 (1) (2000) 711–717.
[77] D. Andrienko, M.P. Allen, Molecular simulation and theory of a liquid crystalline disclination core, Phys. Rev. E 61 (1) (2000) 504–510.
[78] D. Andrienko, G. Germano, M.P. Allen, Computer simulation of topological defects around a colloidal particle or droplet dispersed in a nematic host, Phys. Rev. E 63 (4) (2001) 041701.
[79] D. Andrienko, M.P. Allen, G. Skačej, S. žumer, Defect structures and torque on an elongated colloidal particle immersed in a liquid crystal host, Phys. Rev. E 65 (4) (2002) 041702.
[80] M. Kléman, Points, lines and walls: in liquid crystals, magnetic systems and various ordered media, J. Wiley, Chichester, 1983.
[81] Y. Gu, N.L. Abbott, Observation of Saturn-ring defects around solid microspheres in nematic liquid crystals, Phys. Rev. Lett. 85 (22) (2000) 4719–4722.
[82] H. Stark, Director field configurations around a spherical particle in a nematic liquid crystal, Eur. Phys. J. B 10 (2) (1999) 311–321.
[83] S. Grollau, N.L. Abbott, J.J. de Pablo, Spherical particle immersed in a nematic liquid crystal: effects of confinement on the director field configurations, Phys. Rev. E 67 (1) (2003) 011702.
[84] O.V. Kuksenok, R.W. Ruhwandl, S.V. Shiyanovskii, E.M. Terentjev, Director structure around a colloid particle suspended in a nematic liquid crystal, Phys. Rev. E 54 (5) (1996) 5198–5203.
[85] P. Poulin, H. Stark, T.C. Lubensky, D.A. Weitz, Novel colloidal interactions in anisotropic fluids, Science 275 (5307) (1997) 1770–1773.
[86] H. Stark, Physics of colloidal dispersions in nematic liquid crystals, Phys. Rep. 351 (6) (2001) 387–474.
[87] P. Poulin, V. Cabuil, D.A. Weitz, Direct measurement of colloidal forces in an anisotropic solvent, Phys. Rev. Lett. 79 (24) (1997) 4862–4865.
[88] J. Kotar, M. Vilfan, N. Osterman, D. Babič, M. Čopič, I. Poberaj, Interparticle potential and drag coefficient in nematic colloids, Phys. Rev. Lett. 96 (20) (2006) 207801.
[89] J. Kotar, D. Babič, M. Vilfan, M. Čopič, I. Poberaj, Magneto-optic tweezers studies of interactions in liquid crystal colloids, Mol. Cryst. Liq. Cryst. 450 (1) (2006) 97/[297]–104/[304].
[90] M. Vilfan, N. Osterman, M. Čopič, M. Ravnik, S. žumer, J. Kotar, D. Babič, I. Poberaj, Confinement effect on interparticle potential in nematic colloids, Phys. Rev. Lett. 101 (23) (2008) 237801.
[91] C.M. Noël, G. Bossis, A.-M. Chaze, F. Giulieri, S. Lacis, Measurement of elastic forces between iron colloidal particles in a nematic liquid crystal, Phys. Rev. Lett. 96 (21) (2006) 217801.
[92] T. Kishita, K. Takahashi, M. Ichikawa, J.-i. Fukuda, Y. Kimura, Arrangement dependence of interparticle force in nematic colloids, Phys. Rev. E 81 (1) (2010) 010701.
[93] K. Takahashi, M. Ichikawa, Y. Kimura, Direct measurement of force between colloidal particles in a nematic liquid crystal, J. Phys. Condens. Mater. 20 (7) (2008) 075106.
[94] K. Takahashi, M. Ichikawa, Y. Kimura, Force between colloidal particles in a nematic liquid crystal studied by optical tweezers, Phys. Rev. E 77 (2) (2008) 020703.
[95] S. Ramaswamy, R. Nityananda, V.A. Raghunathan, J. Prost, Power-law forces between particles in a nematic, Mol. Cryst. Liq. Cryst. Sci. Technol. Sect. A. Mol. Cryst. Liq. Cryst. 288 (1) (1996) 175–180.
[96] B.I. Lev, P.M. Tomchuk, Interaction of foreign macrodroplets in a nematic liquid crystal and induced supermolecular structures, Phys. Rev. E 59 (1) (1999) 591–602.
[97] B.I. Lev, S.B. Chernyshuk, P.M. Tomchuk, H. Yokoyama, Symmetry breaking and interaction of colloidal particles in nematic liquid crystals, Phys. Rev. E 65 (2) (2002) 021709.
[98] B.I. Lev, H. Yokoyama, S.B. Chernyshuk, P.M. Tomchuk, Symmetry breaking, elastic interaction and structures in nematic colloids, Mol. Cryst. Liq. Cryst. 409 (1) (2004) 99–109.
[99] O.M. Tovkach, S.B. Chernyshuk, B.I. Lev, Colloidal interactions in a homeotropic nematic cell with different elastic constants, Phys. Rev. E 92 (4) (2015) 042505.
[100] M. Škarabot, M. Ravnik, S. žumer, U. Tkalec, I. Poberaj, D. Babič, N. Osterman, I. Muševič, Two-dimensional dipolar nematic colloidal crystals, Phys. Rev. E 76 (5) (2007) 051406.
[101] J.-i. Fukuda, H. Yokoyama, M. Yoneya, H. Stark, Interaction between particles in a nematic liquid crystal: numerical study using the Landau-de Gennes continuum theory, Mol. Cryst. Liq. Cryst. 435 (1) (2005) 63/[723]–74/[734].
[102] U. Ognysta, A. Nych, V. Nazarenko, I. Muševič, M. Škarabot, M. Ravnik, S. žumer, I. Poberaj, D. Babič, 2D interactions and binary crystals of dipolar and quadrupolar nematic colloids, Phys. Rev. Lett. 100 (21) (2008) 217803.
[103] I.I. Smalyukh, O.D. Lavrentovich, A.N. Kuzmin, A.V. Kachynski, P.N. Prasad, Elasticity-mediated self-organization and colloidal interactions of solid spheres with tangential anchoring in a nematic liquid crystal, Phys. Rev. Lett. 95 (15) (2005) 157801.
[104] M. Škarabot, M. Ravnik, S. žumer, U. Tkalec, I. Poberaj, D. Babič, N. Osterman, I. Muševič, Interactions of quadrupolar nematic colloids, Phys. Rev. E 77 (3) (2008) 031705.
[105] U. Ognysta, A. Nych, V. Nazarenko, M. Škarabot, I. Muševič, Design of 2D binary colloidal crystals in a nematic liquid crystal, Langmuir 25 (20) (2009) 12092–12100.
[106] M. Tasinkevych, D. Andrienko, Colloidal particles in liquid crystal films and at interfaces, Condens. Matter Phys. 13 (3) (2010) 33603.
[107] P. Patrício, M. Tasinkevych, M.M.T.d. Gama, Colloidal dipolar interactions in 2D smectic-C films, Eur. Phys. J. E 7 (2) (2002) 117–122.
[108] K.S. Korolev, D.R. Nelson, Defect-mediated emulsification in two dimensions, Phys. Rev. E 77 (5) (2008) 051702.
[109] C. Zhou, P. Yue, J.J. Feng, Dynamic simulation of droplet interaction and self-assembly in a nematic liquid crystal, Langmuir 24 (7) (2008) 3099–3110.
[110] J.-i. Fukuda, H. Stark, M. Yoneya, H. Yokoyama, Interaction between two spherical particles in a nematic liquid crystal, Phys. Rev. E 69 (4) (2004) 041706.
[111] M. Tasinkevych, N.M. Silvestre, P. Patrício, M.M. Telo da Gama, Colloidal interactions in two-dimensional nematics, Eur. Phys. J. E 9 (4) (2002) 341–347.
[112] O. Guzmán, E.B. Kim, S. Grollau, N.L. Abbott, J.J. de Pablo, Defect structure around two colloids in a liquid crystal, Phys. Rev. Lett. 91 (23) (2003) 235507.
[113] N.M. Silvestre, P. Patrício, M. Tasinkevych, D. Andrienko, M.M. Telo da Gama, Colloidal discs in nematic liquid crystals, J. Phys. Condens. Mater. 16 (19) (2004) S1921.
[114] J.-i. Fukuda, H. Yokoyama, Separation-independent attractive force between like particles mediated by nematic-liquid-crystal distortions, Phys. Rev. Lett. 94 (14) (2005) 148301.
[115] F.R. Hung, Quadrupolar particles in a nematic liquid crystal: effects of particle size and shape, Phys. Rev. E 79 (2) (2009) 021705.
[116] M. Ravnik, S. žumer, Landau–de Gennes modelling of nematic liquid crystal colloids, Liq. Cryst. 36 (10–11) (2009) 1201–1214.
[117] D. Andrienko, M. Tasinkevych, P. Patrício, M.P. Allen, M.M.T. da Gama, Forces between elongated particles in a nematic colloid, Phys. Rev. E 68 (5) (2003) 051702.
[118] D.L. Cheung, M.P. Allen, Liquid-crystal-mediated force between a cylindrical nanoparticle and substrate, Phys. Rev. E 76 (4) (2007) 041706.
[119] D.L. Cheung, M.P. Allen, Forces between cylindrical nanoparticles in a liquid crystal, Langmuir 24 (4) (2008) 1411–1417.
[120] I.I. Smalyukh, S. Chernyshuk, B.I. Lev, A.B. Nych, U. Ognysta, V.G. Nazarenko, O.D. Lavrentovich, Ordered droplet structures at the liquid crystal surface and elastic-capillary colloidal interactions, Phys. Rev. Lett. 93 (11) (2004) 117801.

[121] I.-H. Lin, G.M. Koenig, J.J. de Pablo, N.L. Abbott, Ordering of solid microparticles at liquid crystal-water interfaces, J. Phys. Chem. B 112 (51) (2008) 16552–16558.
[122] G.M. Koenig, I.-H. Lin, N.L. Abbott, Chemoresponsive assemblies of microparticles at liquid crystalline interfaces, Proc. Natl. Acad. Sci. U. S. A. 107 (9) (2010) 3998–4003.
[123] B. Lev, S.B. Chernyshuk, T. Yamamoto, J. Yamamoto, H. Yokoyama, Photochemical switching between colloidal photonic crystals at the nematic-air interface, Phys. Rev. E 78 (2) (2008) 020701.
[124] A.B. Nych, U.M. Ognysta, V.M. Pergamenshchik, B.I. Lev, V.G. Nazarenko, I. Muševič, M. Škarabot, O.D. Lavrentovich, Coexistence of two colloidal crystals at the nematic-liquid-crystal-air interface, Phys. Rev. Lett. 98 (5) (2007) 057801.
[125] V.J. Anderson, E.M. Terentjev, S.P. Meeker, J. Crain, W.C.K. Poon, Cellular solid behaviour of liquid crystal colloids. 1. Phase separation and morphology, Eur. Phys. J. E 4 (1) (2001) 11–20.
[126] M. Roth, M. D'Acunzi, D. Vollmer, G.K. Auernhammer, Viscoelastic rheology of colloid-liquid crystal composites, J. Chem. Phys. 132 (12) (2010) 124702.
[127] V.J. Anderson, E.M. Terentjev, Cellular solid behaviour of liquid crystal colloids. 2. Mechanical properties, Eur. Phys. J. E 4 (1) (2001) 21–28.
[128] J.L. West, A. Glushchenko, G. Liao, Y. Reznikov, D. Andrienko, M.P. Allen, Drag on particles in a nematic suspension by a moving nematic-isotropic interface, Phys. Rev. E 66 (1) (2002) 012702.
[129] J. West*, K. Zhang, A. Glushchenko, Y. Reznikov, D. Andrienko, Drag of micro–particles by an extended nematic-isotropic interface, Mol. Cryst. Liq. Cryst. 422 (1) (2004) 73–82.
[130] J.L. West, K. Zhang, A. Glushchenko, D. Andrienko, M. Tasinkevych, Y. Reznikov, Colloidal particles at a nematic-isotropic interface: effects of confinement, Eur. Phys. J. E 20 (2) (2006) 237–242.
[131] M. Oettel, S. Dietrich, Colloidal interactions at fluid interfaces, Langmuir 24 (4) (2008) 1425–1441.
[132] M. Oettel, A. Domınguez, M. Tasinkevych, S. Dietrich, Effective interactions of colloids on nematic films, Eur. Phys. J. E 28 (2) (2009) 99–111.
[133] D. Andrienko, M. Tasinkevych, P. Patrício, M.M. Telo da Gama, Interaction of colloids with a nematic-isotropic interface, Phys. Rev. E 69 (2) (2004) 021706.
[134] D. Andrienko, M. Tasinkevych, S. Dietrich, Effective pair interactions between colloidal particles at a nematic-isotropic interface, Europhys. Lett. (EPL) 70 (1) (2005) 95.
[135] M. Tasinkevych, D. Andrienko, Effective triplet interactions in nematic colloids, Eur. Phys. J. E 21 (3) (2006) 277–282.
[136] M.R. Wilson, D. Demus, J. Goodby, G.W. Gray, H.-W. Spiess, V. Vill, Molecular modelling, Handbook of Liquid Crystals Set, Wiley-VCH Verlag GmbH. 1998, pp. 72–86.
[137] D.J. Evans, S. Murad, Singularity free algorithm for molecular dynamics simulation of rigid polyatomics, Mol. Phys. 34 (2) (1977) 327–331.
[138] P.S.Y. Cheung, J.G. Powles, The properties of liquid nitrogen, Mol. Phys. 30 (3) (1975) 921–949.
[139] D. Fincham, Leapfrog rotational algorithms for linear molecules, Molecular Simul. 11 (1) (1993) 79–89.
[140] B.J. Berne, P. Pechukas, Gaussian model potentials for molecular interactions, J. Chem. Phys. 56 (8) (1972) 4213–4216.
[141] J.G. Gay, B.J. Berne, Modification of the overlap potential to mimic a linear site–site potential, J. Chem. Phys. 74 (6) (1981) 3316–3319.
[142] M.A. Bates, G.R. Luckhurst, Computer simulation studies of anisotropic systems. XXX. The phase behavior and structure of a Gay–Berne mesogen, J. Chem. Phys. 110 (14) (1999) 7087–7108.
[143] E. de Miguel, L.F. Rull, M.K. Chalam, K.E. Gubbins, Liquid crystal phase diagram of the Gay-Berne fluid, Mol. Phys. 74 (2) (1991) 405–424.
[144] E. de Miguel, L.F. Rull, K.E. Gubbins, Dynamics of the Gay-Berne fluid, Phys. Rev. A 45 (6) (1992) 3813–3822.
[145] R. Berardi, A.P.J. Emerson, C. Zannoni, Monte Carlo investigations of a Gay–Berne liquid crystal, J. Chem. Soc. Faraday Trans. 89 (22) (1993) 4069–4078.
[146] G.R. Luckhurst, R.A. Stephens, R.W. Phippen, Computer simulation studies of anisotropic systems. XIX. Mesophases formed by the Gay-Berne model mesogen, Liq. Cryst. 8 (4) (1990) 451–464.
[147] M.A. Bates, G.R. Luckhurst, Computer simulation studies of anisotropic systems. XXVI. Monte Carlo investigations of a Gay–Berne discotic at constant pressure, J. Chem. Phys. 104 (17) (1996) 6696–6709.
[148] N. Metropolis, S. Ulam, The Monte Carlo method, J. Am. Stat. Assoc. 44 (247) (1949) 335–341.
[149] M.P. Allen, D. Frenkel, Calculation of liquid-crystal Frank constants by computer simulation, Phys. Rev. A Gen. Phys. 37 (5) (1988) 1813–1816.
[150] D.J. Cleaver, M.P. Allen, Computer simulations of the elastic properties of liquid crystals, Phys. Rev. A 43 (4) (1991) 1918–1931.
[151] N.H. Phuong, G. Germano, F. Schmid, Elastic constants from direct correlation functions in nematic liquid crystals: a computer simulation study, J. Chem. Phys. 115 (15) (2001) 7227–7234.
[152] J. Stelzer, L. Longa, H.-R. Trebin, Elastic constants of nematic liquid crystals from molecular dynamics simulations, Molecular Crystals and Liquid Crystals Science and Technology. Section A, Mol. Cryst. Liq. Cryst. Sci. Technol. Sect. A Mol. Cryst. Liq. Cryst. 262 (1) (1995) 455–461.
[153] J. Stelzer, L. Longa, H.-R. Trebin, Molecular dynamics simulations of a Gay–Berne nematic liquid crystal: elastic properties from direct correlation functions, J. Chem. Phys. 103 (8) (1995) 3098–3107.
[154] D. Baalss, S. Hess, Nonequilibrium molecular-dynamics studies on the anisotropic viscosity of perfectly aligned nematic liquid crystals, Phys. Rev. Lett. 57 (1) (1986) 86–89.
[155] S. Sarman, Flow properties of liquid crystal phases of the Gay–Berne fluid, J. Chem. Phys. 108 (18) (1998) 7909–7916.
[156] M.P. Allen, Simulation of condensed phases using the distributed array processor, Theor. Chim. Acta 84 (4–5) (1993) 399–411.
[157] R. Memmer, F. Janssen, Computer simulation of chiral liquid crystal phases, J. Chem. Soc. Faraday Trans. 94 (2) (1998) 267–276.
[158] M.P. Allen, Molecular simulation and theory of the isotropic–nematic interface, J. Chem. Phys. 112 (12) (2000) 5447–5453.
[159] S.D. Hudson, R.G. Larson, Monte Carlo simulation of a disclination core in nematic solutions of rodlike molecules, Phys. Rev. Lett. 70 (19) (1993) 2916–2919.
[160] H. Kawamoto, The history of liquid-crystal displays, Proc. IEEE 90 (4) (2002) 460–500.
[161] D.-K. Yang, S.-T. Wu, Fundamentals of Liquid Crystal Devices, 2nd edition ed., Wiley, Chichester, West Sussex, United Kingdom, 2014.
[162] J.P.F. Lagerwall, G. Scalia, A new era for liquid crystal research: applications of liquid crystals in soft matter nano-, bio- and microtechnology, Curr. Appl. Phys. 12 (6) (2012) 1387–1412.